https://doi.org/10.1070/RCR5044

Supercapacitors: problems and prospects of development

Yury M. Volfkovich

Frumkin Institute of Physical Chemistry and Electrochemistry, Russian Academy of Sciences, 31 Leninsky prosp., 119991 Moscow, Russian Federation

The review describes the design of supercapacitors and demonstrates their advantages over batteries and their main drawback: fast self-discharge. Various types of highly dispersed carbon materials for electrodes, functional groups on their surface, porous structure and hydrophilic–hydrophobic properties are considered. Data on the self-discharge of supercapacitors are discussed. Self-discharge investigation methods, mechanisms and mathematical modelling are analyzed and the effect of surface functional groups on this process is demonstrated. The methods for minimizing the self-discharge are described, in particular, using additives to the electrolyte, design of solid-state supercapacitors and supercapacitors with ion exchange membranes, the use of electrolytes free from impurities and chemical modification of electrodes. The developed new-generation supercapacitors with enhanced characteristics are mentioned. Electrodes based on conductive polymers are considered, and the key characteristics of supercapacitors manufactured by various companies are given.
The bibliography includes 160 references.

Contents

1. Introduction 1
2. Structure of supercapacitors 2
3. Advantages of supercapacitors over batteries 2
4. Main drawback of supercapacitors 2
5. Main properties of supercapacitors 3
6. Highly dispersed carbon electrodes 5
   6.1. Activated carbons 5
   6.2. Templated porous carbon 5
   6.3. Carbide carbons 6
   6.4. Carbon aerogels 6
   6.5. Carbon nanotubes 6
   6.6. Graphene and its derivatives 6
7. Functional groups on the surface of highly dispersed carbon materials 7
8. Porous structure and hydrophilic–hydrophobic properties of highly dispersed carbon electrodes 8
9. Study of the self-discharge of supercapacitors 9
   9.1. Investigation methods 9
   9.2. Self-discharge mechanisms 10
   9.3. Mathematical modelling of self-discharge 11
10. Development of new supercapacitors with enhanced characteristics 12
   10.1. Use of special additives to the electrolyte 12
   10.2. Solid-state supercapacitors 12
   10.3. Supercapacitors with ion exchange membranes 13
   10.4. Use of electrolytes free from impurities 13
   10.5. Methods of chemical modification of electrodes to suppress self-discharge 14
   10.6. Hybrid supercapacitors 14
   10.7. Development of new supercapacitors 14
11. Conclusion 16
12. List of abbreviations and symbols 17
13. References 17

1. Introduction

According to generally accepted definition, which was first formulated by Conway,[1] supercapacitors (SCs) are devices in which quasi-reversible electrochemical charge–discharge processes take place. The shape of galvanostatic curves is nearly linear, *i.e.*, resembles the shape of such curves observed for usual electrostatic capacitors. Highly dispersed carbon materials (HDCMs) are used most often to fabricate SCs.[2–13]

Yu.M.Volfkovich. Doctor of Chemical Sciences, Chief Researcher at IPCE RAS.
E-mail: yuvolf40@mail.ru
Current research interests: electrochemical energy (supercapacitors, fuel cells, batteries), water desalination by capacitive deionization, porosimetry.
Translation: Z.P.Svitanko

Supercapacitor are classified into electrical double-layer capacitors (EDLCs),[1,14] pseudocapacitors (PsC)[1,14] and hybrid supercapacitors (HSCs).[1,14] The double-layer SCs based on charging of the electrical double layer (EDL) contain HDCMs-based electrodes. At the PsC electrodes, fast quasi-reversible Faradaic processes take place. As a rule, the capacitance of PsC electrodes is higher than that of EDLC electrodes. The PsC electrodes are classified into three main types:

— electrodes based on inorganic transition metal compounds (oxides, sulfides, nitrides, *etc.*);

— electrodes based on electrically conductive polymers (ECPs); such polymers are used most often;

— electrodes based on monomeric redox systems.

All PsCs correspond to the above definition by Conway.[1] In hybrid supercapacitors, electrodes of different types are used, *e.g.*, one HDCM electrode and one ECP or battery electrode. It should be noted that PsCs and HSCs

Received 16 January 2022

© 2022 Uspekhi Khimii, ZIOC RAS, Russian Academy of Sciences

are usually characterized by higher energy density, but lower power density than EDLCs.

In 1957, General Electric patented the first EDLC, which consisted of porous carbon electrodes and used EDL capacitance for charging. The Standard Oil Company (SOHIO) in Ohio, USA, patented a device that stored energy in the EDL at the electrode/solution interface. The Japanese Nippon Electric Company (NEC) received a license from SOHIO for manufacturing and presented the first EDLC in the market in 1957. The double-layer capacitors patented by SOHIO in 1970 were disc-shaped and consisted of carbon paste impregnated with electrolyte. The first commercially successful EDLC was manufactured by NEC. Several companies commenced the manufacture of SCs by the 1980s. The first EDLCs in the USSR were designed by All-Union Research Institute of Current Sources in the 1970s.[14] The significance of the development of SCs is confirmed in recent reviews (*e.g.* Refs 2–13).

Supercapacitors with very broad range of charge–discharge times (from fractions of a second to several hours) are used in various devices; they are classified into two main types — power type (or pulsed) SCs possessing high power density and energy type SCs possessing high energy density. Each type of SCs has its own applications — for electric vehicles, motor vehicles, locomotives (for the start-up of internal combustion engines) and in various electronic devices. In electric vehicles, SCs can be used together with fuel cells for the boost mode. The key applications of SCs are as follows: electrical energy storage and release to balance the peak loads in electrical networks; recovery of braking energy of internal combustion engines (in motor vehicles, locomotives, aircrafts, ships); energy redundancy in railway, underground and other types of public transport; creation of large buffer energy storages in electrical power engineering, telecommunication systems, uninterruptible power supply systems; alternative electrical power engineering, battery replacement in substations; and meeting peak power demand.

2. Structure of supercapacitors

An electrical double-layer SC is an electrochemical cell with a porous separator and polarizable electrodes based on HDCMs with a large (of the order of 500–2500 $m^2\ g^{-1}$) specific surface area contacting with the separator on both sides. The cell pores are impregnated with an aqueous or non-aqueous electrolyte. In EDLC, quasi-reversible charge–discharge electrochemical processes take place.[1,2] The electrodes are fabricated using materials with diverse porous structures and hydrophilic–hydrophobic properties: activated carbons (AC), carbon nanotubes (CNTs), graphene, carbon blacks, aerogels, xerogels and so on. Almost every carbon material contains both hydrophilic and hydrophobic pores, which considerably affects electrochemical characteristics of SCs with aqueous electrolytes.[15] It is also known that HDCMs have a variety of surface functional groups (SFGs), which change the electrochemical characteristics of SCs such as capacitance, energy and power. The major contribution to the capacitance of EDLCs is made by the EDL capacitance. In some cases, some contribution comes from the pseudocapacitance of Faradaic redox reactions involving SFGs; the pseudocapacitance of EDLCs is very low.

3. Advantages of supercapacitors over batteries

The industrial manufacture of supercapacitors is now rapidly increasing, which stimulates relevant studies and opens up new fields of practical application of SCs.[1,2] Supercapacitors have numerous advantages over traditional rechargeable electrochemical energy sources such as batteries. These advantages include markedly longer operating time, an almost unlimited cyclability (from hundreds of thousands to a million of cycles, while the batteries withstand only several hundred or thousand cycles), markedly higher specific power, relatively low cost, operation over broad ranges of charge–discharge times and temperatures, environmental friendliness and theoretically attainable almost 100% energy efficiency (discharge energy to charge energy ratio). The last-mentioned issue is implemented in the case of practically predominant contribution of EDL capacitance to the total capacitance of SCs, which is true for EDLCs.[16] The energy efficiency of batteries is markedly restricted by polarization of electrode reactions due to relatively low exchange currents. The possibility of attaining an energy efficiency approaching 100% opens up prospects of SC application for leveling the peak loads of electrical networks.

An important benefit of SCs is the possibility of using them for water desalination by the capacitive deionization method. In this method, electrochemical cells of the same type with two HDCM-based electrodes with a specific surface area of 500–2500 $m^2\ g^{-1}$ are used.[17,18] The capacitive deionization of water is associated with lower energy expenditures than all other desalination methods, including the most popular reverse osmosis process.

4. Main drawback of supercapacitors

A considerable drawback of SCs is their significant self-discharge — decrease in the voltage and the amount of stored energy after charging and disconnection of the external circuit.[1] The authors of the vast majority of publications devoted to SCs (there are many thousands of such publications) do not mention self-discharge for promotion purposes; therefore, it is very important to systematically investigate this adverse phenomenon and to elaborate measures that would suppress the self-discharge and, hence, contribute to expansion of the scope of applicability of SCs. This review is to a large extent devoted to such investigations.

It was suggested[19,20] that the self-discharge phenomenon attests to a non-equilibrium state of SC, which tends to reach thermodynamic equilibrium. The authors concluded that self-discharge is an inevitable problem for supercapacitors with carbon electrodes. Kowal *et al.*[21] found that 5 to 60% of the voltage is lost within two weeks and that the self-discharge rate depends on a number of factors such as the initial voltage, temperature, charging time and prehistory.

The self-discharge curves — dependences of the change in the voltage (U) on time (t) for various initial voltages — for commercial Supercup SCs with an acetonitrile electrolyte are shown in Fig. 1.[21] It can be seen that the rate of voltage decay over time after opening the electrical circuit, which characterizes self-discharge, increases with increasing initial voltage. On the basis of experimental studies, Kowal

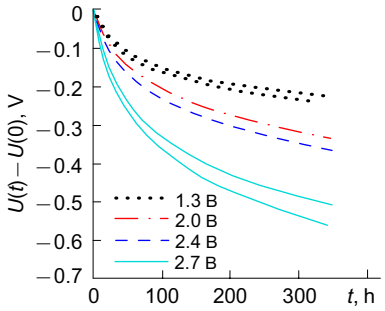


Figure 1. Time dependence of the $U(t)-U(0)$ difference for commercial Supercup SC with acetonitrile electrolyte. $U(0)$ is the initial voltage, $U(t)$ is the current voltage. For $U(0) = 1.3$ and 2.7 V, two measurements were carried out.[21] Published with permission from Elsevier.

et al.[21] developed a simple mathematical model to interpret the mechanisms of voltage decay and leakage current and demonstrated that self-discharge increases with temperature rise.

5. Main properties of supercapacitors

Electrical double-layer capacitors are based on porous polarizable carbon electrodes. The energy storage in EDLCs is due to charge separation on the two electrodes when there is a large potential difference between them. The electrical charge of EDLC is determined by the EDL capacitance. During charging, electrons migrate from the positive electrode to the negative one *via* the external current source. The ions present in the electrolyte bulk move towards the electrodes. During the discharge, electrons move from the negative electrode to the positive one across a load resistor, while the ions return to the electrolyte bulk. The charging and discharging processes are accompanied by changes in the charge density at the interface and the electrolyte concentration. The theoretical views of the specific (per unit true electrode surface) capacitance of EDL are based on known classical Helmholtz, Stern, Gouy–Chapman, Graham and other theories.

For detailed electrochemical analysis of SC electrodes, like for other electrochemical systems, cyclic voltammetry (CV) is used, that is, current *vs.* potential curves are recorded at a specified potential sweep rate (V s^{-1}). In the first approximation, CV curve for an ideal EDLC, in which only EDL charge–discharge processes take place, is a rectangle with the sides being parallel and perpendicular to the abscissa axis.

Like for any ideal capacitor, the capacitance (C) of EDLC is inversely proportional to the plate thickness (d)

$$C = \frac{\ni}{4\pi d} \tag{1}$$

where ∋ is the dielectric constant of the electrolyte. For example, the plate of a classical paper capacitor is an interlayer between the electrodes, which is several tens of micrometres thick. Therefore, such capacitors have low specific capacitance. In the case of EDLCs, the plate thickness is equal to EDL thickness, which is several tenths of a nanometre. Hence, the specific capacitance of EDLCs per unit true electrode/liquid electrolyte interfacial area (C_s) is many orders of magnitude higher than that of conventional capacitors; for example, for aqueous electrolytes C_s is 10–20 μF cm^{-2}, while for non-aqueous electrolytes, it is several microfarads per square centimetre. This is a significant advantage of EDLCs over paper capacitors.

The capacitance per unit mass of a porous electrode of EDLCs (C_g) is determined from the formula

$$C_g = C_s S \tag{2}$$

(S is the specific surface area, m^2 g^{-1}); therefore, to attain a high capacitance for EDLCs, electrodes based on HDCMs with a high specific surface area (500–2500 m^2 g^{-1}) are used.

For EDLCs with ideal polarizable electrodes, the discharge energy density (A) is equal to [1]

$$A = \frac{1}{2} C (U_{max}^2 - U_{min}^2) \tag{3}$$

where C is the specific capacitance of the electrodes, U_{max} and U_{min} are the initial and final discharge voltages. If $U_{min} = 0$, then

$$A = A_{max} = \frac{1}{2} C U_{max}^2 \tag{4}$$

Due to low solubility of non-aqueous electrolytes, the energy density of EDLCs depends not only on the capacitance, but also on the electrolyte concentration.

It can be seen from Eqn (4) that the maximum discharge energy density for EDLCs is directly proportional to the capacitance and to the maximum voltage squared. While comparing the energy density for EDLCs with aqueous and non-aqueous electrolytes, one should bear in mind that in the case of aqueous electrolytes, the specific capacitance and electrical conductivity values are higher, while the maximum voltage is lower than these values for non-aqueous electrolytes. The dependences of the discharge energy (A) on the discharge current density (i) measured for symmetrical EDLC with identical electrodes based on activated carbon cloth with $S = 600$ m^2 g^{-1} with aqueous and non-aqueous electrolytes are shown in Fig. 2.[19] It can be seen that at low current densities, the energy density is higher for EDLC with non-aqueous electrolyte, while at high current densities, it is higher for EDLC with aqueous electrolyte.

There are two approaches to calculation of the peak power density of EDLCs and batteries.[2] The first (standard) approach is to determine the power for the impedance state at which half of the discharge energy is converted to electricity and the other half is converted to heat (the discharge efficiency is 60%). The maximum power density at this time instant (P_{mi}) is determined by the equation

$$P_{mi} = \frac{U_{oc}^2}{4R_b} \tag{5}$$

where U_{oc} is the maximum voltage of SC or open circuit voltage of a battery, R_b is the resistance of the corresponding device.

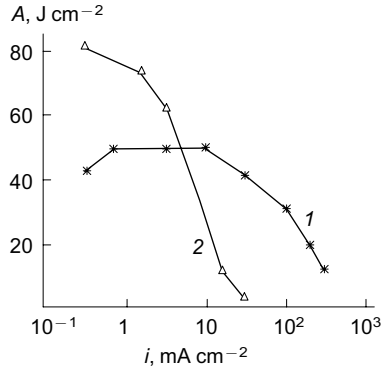


Figure 2. Energy density *vs.* discharge current density for EDLCs with aqueous (*1*) and non-aqueous (*2*) electrolytes. (*1*) 35% H_2SO_4, (*2*) 1 M $LiAlF_4$ + γ-butyrolactone.[19] Published with permission from Springer.

The efficiency of charge–discharge cycles is highly significant for many applications in which a considerable fraction of energy is stored in an energy storage system.[22, 23] In these cases, the use of an energy storage system should be restricted to conditions providing high efficiency of charge and discharge processes. The charge–discharge power of SC or battery (P_{ef}) as a function of performance is determined by the equation

$$P_{ef} = EF(1-EF)\frac{U_{oc}^2}{R_b} \quad (6)$$

where EF is the pulse efficiency. When EF = 0.95, one has $P_{ef}/P_{mi} = 0.19$. Thus, for applications where the main goal is to reach high efficiency, useful power of EDLC or a battery is much lower than the peak power, which is most often indicated by the manufacturer of the device. In the case of EDLCs, the peak power density (P_{pi}) during discharge from the rated voltage U_0 down to $U_0/2$ is determined by the following formula:[2]

$$P_{pi} = \frac{9}{16}(1-EF)\frac{U_{oc}^2}{R_{uc}} \quad (7)$$

where R_{uc} is the resistance of EDLC. This equation takes account for the decrease in the voltage during the discharge. It is evident that in most cases, the EDLC power is higher than the power of a battery. Experience showed that double-layer supercapacitors that had not been used for several years were still almost in the initial operating state; EDLCs can be cycled at high rates (discharge over seconds) for hundreds of thousands or millions of cycles, with the change in the characteristics being moderate during this period (10–20% degradation of the capacitance and resistance). This is impossible in the case of batteries, even if the depth of discharge is relatively low (10–20%).

The difference ($U_{max} - U_{min}$) is called the potential window. The greater this window, the higher the EDLC energy density and power density. The use of non-aqueous electrolytes in EDLCs expands the potential window (up to 3–3.5 V), which would considerably increase both the energy density [see Eqn (4)] and power density [see Eqn (7)]. However, some factors act in the opposite direction, namely, the specific capacitance decreases (because of the greater size of solvent molecules compared to the size of micropores) and the electrical conductivity also decreases compared to that for aqueous electrolytes. Concentrated aqueous solutions of H_2SO_4 and KOH have high electrical conductivity, which makes it possible to attain high power; however, the energy performance characteristics of EDLCs decrease due to narrow operating voltage range (~1 V). Finally, the optimal conditions for attaining higher specific power should be selected in each particular case.

Unlike batteries, supercapacitors can function over a very broad range of charge and discharge times (from fractions of a second to several hours). Accordingly, as noted above, SCs are classified into two main types:

— power type (high power density),

— energy type (high energy density).

In the case of power type supercapacitors, including EDLCs, it is possible to carry out the charge–discharge processes over short periods of time and, when concentrated aqueous electrolytes are used, to attain high power density (up to several tens of kW per kg). Measurements for HDCM-based electrodes in the operation modes of energy type SCs usually give specific capacitance values in the range from 50 to 200 F g^{-1}. The highest specific capacitance of 320 F g^{-1} was attained owing to a considerable contribution of the pseudocapacitance from quasireversible redox reactions of SFGs. Thus, it is no longer an ideal EDLCs.

The Ragone plots illustrating the broad range of characteristic charge–discharge times for various rechargeable electrochemical devices, that is, lead, nickel metal hydride and lithium ion batteries, as well as electrolytic capacitors and SCs are shown in Fig. 3. The functioning regions of these devices are depicted in the specific power–specific energy coordinates.[10]

It can be seen that the time range of functioning of a supercapacitor extends over 7 orders of magnitude, which is much longer than the time range of functioning of a battery. Supercapacitors have lower specific energy, but much higher specific power than batteries.

Since a porous electrode of EDLC is ideally polarized, the main processes that occur during operation include non-stationary charging of EDL at the electrode/electrolyte interface in the pores, diffusion-migration ion transport in the electrolyte and processes responsible for the ohmic loss of energy. According to the theory of porous electrodes, the potential (E) distribution across the electrode thickness (*i.e.*, along the x coordinate) is described by the following equation:[24]

$$\kappa\frac{\partial^2 E}{\partial x^2} = Si(E) \quad (8)$$

where κ is the effective conductivity of the electrolyte in the pores, S is the specific surface area of the electrode ($cm^2\,cm^{-3}$), $i(E)$ is the dependence of the local current density at the interface on the potential. The current density is determined by charging (discharging) of EDL

$$i = C_s\frac{\partial E}{\partial t} \quad (9)$$

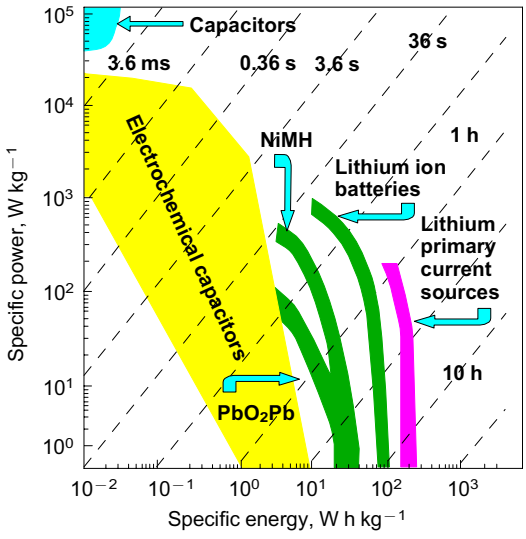


Figure 3. Ragone plots for various rechargeable electrochemical devices.[10] Published with permission from Springer.

where C_s is the EDL specific capacitance per unit surface area, t is time. In the galvanostatic mode, the boundary and initial conditions for Eqns (8) and (9) have the form

$$E_{(x,\ t=0)} = E_0 \tag{10}$$

$$I = \kappa \left(\frac{\partial E}{\partial x}\right)_{x=L} \tag{10a}$$

$$\left(\frac{\partial E}{\partial x}\right)_{x=0} = 0 \tag{10b}$$

where I is the current density per unit of external surface of the electrode. Volfkovich *et al.*[25] proposed the first analytical solution for system of equations (8)–(10b) and compared the results with experimental charge–discharge curves for symmetrical EDLCs with two identical electrodes made of AUT-600 cloth with aqueous (10 M KOH) and non-aqueous (1 M $LiAlF_4$ + γ-butyrolactone) electrolytes. The theoretical and experimental curves were in good agreement, which attested to adequacy of this model as applied to EDLCs.

6. Highly dispersed carbon electrodes

6.1. Activated carbons

Activated carbons are among the most popular materials for SCs and are described in numerous publications.[1–3, 5–7, 10, 15, 16, 18, 19, 25–33] Activated carbons are obtained by carbonization followed by activation of many natural and synthetic carbonaceous materials. They are produced from plant and animal feedstock (wood, nut shells, fruit pits, sugar, coconut, bones, *etc.*), mineral raw materials (coal, pitch, peat, tar, coke), synthetic resins and polymers. During carbonization, the starting compounds (precursors) decompose and non-carbon components are removed. Gas-phase activation with steam, carbon dioxide or oxygen at 500–900 °C results in oxidation and partial burning out of carbon and elementary crystallites, which gives rise to the extensive porous structure of activated carbon. Liquid-phase activation with alkalis or nitric acid is also used. Depending on the AC production process, the Brunauer–Emmett–Teller (BET) specific surface area (S_{BET}) varies over a very broad range: from ~500 to 2500 $m^2\ g^{-1}$. The structure of AC comprises micro-, meso- and macropores; the greatest contribution to the specific surface area is made by micropores, which is followed by mesopores.

If a plant raw material is used as the precursor, the resulting AC contains inorganic impurities (ash), which are responsible for the self-discharge of SCs (see below). Ash is removed by treating AC with concentrated acids. The activation with simultaneous change in the porous structure gives rise to functional groups on the AC surface and modifies the electrophysical characteristics. The chemical composition of the carbon surface and the porous structure and electrophysical characteristics of AC significantly affect the electrochemical properties of SCs. The EDL capacitance is usually in the range from 50 to 200 $F\ g^{-1}$. It is known that the SC capacitance decreases with increasing rate of charge–discharge processes.

Electrodes made of CH900 (Kuraray Co, Japan) and TSA (Research and Production Association 'Neorganika', Electrostral, Russia) AC clothes were cycled[32, 33] in the maximum potential range from −1 to 1 V *versus* reversible hydrogen electrode (RHE) due to high overvoltage of hydrogen evolution on carbon. For more convenient representation of capacitance characteristics, especially those measured at different potential sweep rates (w), CV data were depicted as cyclic capacitance–voltage ($C-E$) curves

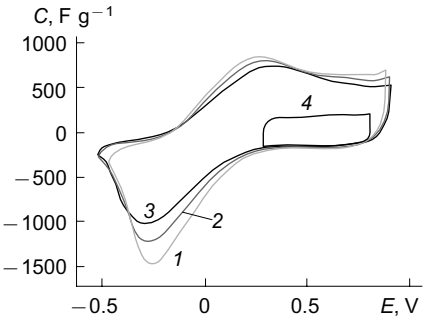
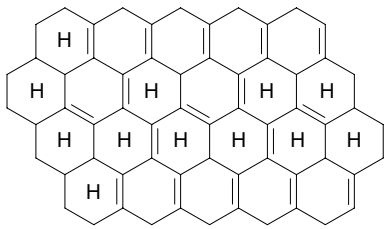


Figure 4. Cyclic capacitance-*vs.*-voltage curves for the CH900 AC cloth; w, $mV\ s^{-1}$: (*1*) 0.5; (*2*) 1.0; (*3*, *4*) 2.0.[10] Published with permission from Springer.

$$C = \frac{I\mathrm{d}t}{\mathrm{d}E} = \frac{I}{w}$$

where C is the differential capacitance. For the CH900 AC cloth, Figure 4 shows the cyclic capacitance–voltage curves measured in 48.5% H_2SO_4 at various w in two potential regions: reversibility region (0.25–0.8 V) and deep cathodic charging region (from −0.5 to 0.8 V). It can be seen that in the reversibility region, only charging of EDL with a capacitance of 170 $F\ g^{-1}$ takes place in the system (curve *4*). In the charging region at negative potentials (< −0.1 V) (curves *1*–*3*), Faradaic processes with a very high pseudocapacitance take place. It is shown that upon this deep cathodic charging, hydrogen is intercalated into carbon to give C_xH (in the limit, C_6H — hydrogen carbide or carbon hydride). The maximum specific charge equal to 1560 $C\ g^{-1}$ (which corresponds to the specific capacitance of 1110 $F\ g^{-1}$) was attained after charging for 22 h at a potential of −0.31 V *vs.* RHE in 56.4% H_2SO_4. The specific charge during EDL charging was 240 $C\ g^{-1}$. The difference 1560 − 240 amounts to 1320 $C\ g^{-1}$. According to the Faraday law, exactly 1320 $C\ g^{-1}$ should be spent to obtain C_6H; this proves that the limiting cathodic charging of AC actually gives previously unknown structure **1**.

Structure 1



1

6.2. Templated porous carbon

Template method is used to produce both micro- and mesoporous carbons, depending on the template and raw material used.[26–34] The method includes impregnation of a finely porous precursor with an organic solvent (*e.g.*, furfuryl alcohol), carbonization in small pores and dissolution of the precursor. Using various zeolites as the precursors, microporous zeolite-templated carbons (ZTC) were prepared, in particular the carbon with the highest S_{BET} of 4000 $m^2\ g^{-1}$ and specific pore volume of 1.8 $cm^3\ g^{-1}$. Since pores in ZTC were inherited from regular zeolite channels,

they included micropores uniform in both size and morphology and a small portion of mesopores. The CV curves of ZTC in a non-aqueous electrolyte were not rectangular, which pointed to a contribution of pseudocapacitance mainly caused by the presence of oxygen-containing SFGs. Most ZTC showed very high charge–discharge rates, *i.e.*, they had nearly constant capacitance even at high current density of 2 A g^{-1}.

6.3. Carbide carbons

The thermal treatment of carbides (SiC, TiC, B_4C and so on) at temperatures of 400–1200 °C in a chlorine flow leads to dissolution of metals and silicon and gives rise to microporous carbons with $S_{BET} = 1000–2000$ m^2 g^{-1} (Ref. 35). The porous structure of these carbons considerably depends on the precursor and the temperature of treatment. Below 800 °C, micropores are mainly formed but on heating to >800 °C, mesopores start to predominate; for many carbons, S_{BET} reaches a maximum at 800 °C. Using these microporous carbide carbons, SCs were fabricated and studied in various electrolytes.

Carbons based on TiC were obtained at 500–1000 °C; the average size of their micropores and S_{BET} varied from 0.7 to 1.1 nm and from 1000 to 1600 m^2 g^{-1}, respectively. Carbons based on B_4C proved to be efficient for SC with KOH electrolyte. Analysis of the capacitances of SiC-based carbons KU-600C and KU-1500C in an ionic liquid over a broad range of potentials showed that mean-integrated specific capacitance is roughly proportional to the specific surface area. Ariyanto *et al.*[36] synthesized TiC-based carbons using a nickel catalyst. The porosity of the carbide-based carbon was controlled by varying the catalyst weight. For SCs with TiC-based electrodes in a 1 M solution of tetraethylammonium tetrafluoroborate ($TEABF_4$) in acetonitrile at low and very high current densities, specific capacitances of 116 (for 5 mA g^{-1}) and 80 F g^{-1} (for 100 A g^{-1}) were found. In recent years, WC has been used as a precursor for carbide carbons. Testing of SCs obtained in this way in 1 M H_2SO_4 showed a high specific capacitance of 477 F g^{-1} (Ref. 37).

6.4. Carbon aerogels

Aerogels are gels in which the liquid phase has been completely replaced by a gas. These materials have a record-low density and a number of unique properties: hardness, heat resistance, transparency, exceptionally low thermal conductivity, *etc*. As a rule, their bulk porosity reaches 90–99% and the density varies from 150 to 1 mg cm^{-3}. The conditions of preparation of carbon aerogels have a pronounced effect on the SC capacitance.[26,38]

X.Yang *et al.*[38] prepared aerogel by, first, dissolving bamboo fibres in aqueous NaOH–urea solutions and, second, keeping the gel at −20 °C for 12 h with subsequent immersion into a regeneration bath with pure water. Then the cellulose hydrogel was frozen in liquid nitrogen for 48 h. Calcination included heating aerogels to 700, 800, 900 and 1000 °C in an argon flow. After this carbonization procedure, the aerogels were activated with an aqueous solution of KOH. The density of the resulting samples was 10–20 mg cm^{-3} and a specific surface area was 920–1085 m^2 g^{-1}. In a supercapacitor with aerogel electrodes in 6 M KOH, high capacitance equal to 381 F g^{-1} was attained.

Volfkovich *et al.*[39] developed aerogel granules based on reduced graphene oxide (rGO). The external surface of the granules was superhydrophobic, while the internal surface was superhydrophilic.

6.5. Carbon nanotubes

Carbon nanotubes are very promising as electrode materials for supercapacitors.[40–46] The distinctive features of CNTs include large open surface area, separate spaces for storage of electrolyte ions and also high electrical conductivity. The outer surface of CNT walls is mainly the basal plane of graphite. Owing to pronounced polarization and wide potential window, this ideal surface provides a high EDL capacitance. Most CNTs are connected to one another by van der Waals forces; as a result, only the outer tubes in a bundle are exposed to the electrolyte. The EDL is formed on the outer surface of CNTs. Electrolyte ions can also penetrate into the inner space of nanotubes; however, there are the following restrictions: first, most of solvated ions cannot fit into nanotubes because of their very small inner diameter (1.3–1.6 nm); second, aqueous electrolytes do not wet the inner surfaces of nanotubes, as they are hydrophobic.

An EDLC based on single-walled CNTs (SWCNTs) in a sulfuric acid electrolyte showed high power density, namely >20 kW kg^{-1} at very high current densities (up to several hundred amperes per gram).[40] This is due to the regular pore structure, *i.e.*, the absence of tortuosity. In order to use the inner surface of SWCNTs, the tube ends were opened *via* oxidation. If the inner surface of open SWCNTs can be fully used for EDL formation, the limiting capacitance should double. Optimization of the oxidation process of super-SWCNTs resulted in S_{BET} >2000 m^2 g^{-1}, while SCs using $TEABF_4$/PC (PC is propylene carbonate) showed a very high energy density (24.7 W h kg^{-1}) and power density (98.9 kW kg^{-1}). However, high cost is a considerable drawback of SWCNTs, which restricts their broad use.

The number of publications devoted to the properties of SCs based on double-walled CNTs is much smaller than that for SWCNTs, since pure double-walled CNTs are very difficult to prepare. In addition, double- and multi-walled CNTs have lower surface area than SWCNTs.[26,43,44] However, there are numerous publications on the capacitance of multi-walled CNTs, as they are synthesized more easily and they are less expensive than SWCNTs.[26,47] Depending on the methods of synthesis and modification, various types of multi-walled CNTs with various specific surface areas were prepared. Their specific capacitances in the presence of aqueous and non-aqueous electrolytes were in the range from 10 to 100 F g^{-1}, which is lower compared to that of AC. In recent years, CNTs have been also used in SCs as conductive additives to non-conductive metal oxides or to some conductive polymers.[42,44]

6.6. Graphene and its derivatives

In the last decade, graphene and its derivatives have started to be used as electrode materials for supercapacitors.[47–64] Graphene, a two-dimensional allotrope of carbon, was obtained only ~15 years ago. In 2010, the Nobel Prize in physics was awarded for the innovative experiments on this carbon allotrope. The remarkable behaviour of graphene was immediately noticed; this opened up broad opportunities for using graphene in various branches of economy, in particular, in chemical current sources such as supercapacitors. A single layer of graphene sheet has a specific surface area accessible for electrolyte of up to 2675 m^2 g^{-1} (for comparison, the specific surface area of one SWCNT

is, on average, ~1300 $m^2 g^{-1}$). Several single graphene layers form aggregated plates and, as a result, the surface accessible for the electrolyte decreases. Nevertheless, good results for SCs with graphene electrodes have been obtained in recent years. The reduction of carbon leads to material exfoliation and, hence, the volume of the material increases by a large factor.

Reduced graphene oxide (rGO) is prepared by modified Hummers method.[49] It is an electrically conducting powder consisting of plate-like particles, each comprising 2 to 10 graphene monolayers; the particle size varies from 1 to 10 μm in the lateral direction. These plates are grouped into agglomerates that are separated by pores with a broad (4–5 orders of magnitude) range of sizes — micro-, meso- and macropores.[52,63] Reduced graphene oxide-based electrodes possess high reversibility of charge–discharge processes. This can be clearly seen in Fig. 5, which shows the dependences of the specific capacitance on the current density and on the number of galvanostatic charge–discharge cycles for two different rGO-based electrodes with specific surface areas of 450 and 520 $m^2 g^{-1}$. Reduced graphene oxide was deposited on nickel felt;[10] the capacitance was measured in a 30 mass % solution of KOH. It can be seen that, first, the capacitance barely changed as the current density changed by an order of magnitude; second, the capacitance was virtually invariable during 500 galvanostatic cycles. These properties are highly valuable.

Mohammadi *et al.*[61] prepared nanocomposites based on Co_3S_4 particles wrapped in CNT/rGO nanosheets. The rGO100-CNT50-Co_3S_4 system was used as the optimal electrode. This SC showed excellent performance — ultrahigh specific capacitance at a relatively high current density; it also demonstrated an excellent rate capability of 63% after the current density increased 40-fold; in this case, the highest energy density and power density were attained (for details, see Section 10.7 below).

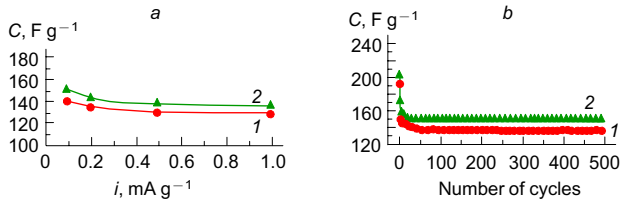
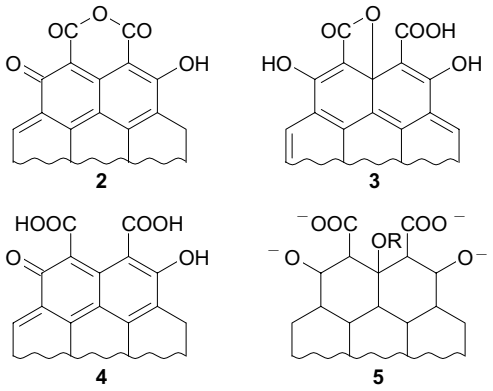


Figure 5. Dependences of specific capacitance on the current density (*a*) and on the number of charge–discharge cycles at a current density of 0.1 $A g^{-1}$ (*b*) for supercapacitors with rGO electrodes with specific surface areas of 450 (*1*) and 520 $m^2 g^{-1}$ (*2*).[10] Published with permission from Springer.

7. Functional groups on the surface of highly dispersed carbon materials

It is known that activated carbons have functional groups on the surface (SFGs; see, for example, **2**–**5**), which are incorporated in the six-membered carbon rings of the activated carbons.[65–67] Data on the surface chemistry of the AG-3 and SCsT-6A active carbons were obtained using the standardized Boehm method.[68–70] It was found that basic groups predominate on the surface of these carbons, with the number of these groups being twice higher on SCsT-6A than on AG-3. The SCsT-6A carbon contains no

Structures 2–5

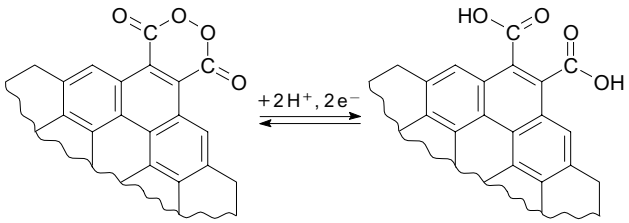


phenol groups, while AG-3 contains no carboxyl or phenol groups.

Tarkovskaya[67] measured the concentrations of hydroxyl, carboxyl and lactone SFGs of the initial and oxidized Norit DLCSupra-30 active carbons. The oxidation of AC was accompanied by a considerable increase in the content of SFGs (mainly hydroxyl groups). The presence of the surface functional groups in the highly dispersed carbon materials of EDLC electrodes influenced the interfacial electrochemistry of the carbon surface and the properties of EDL, particularly, the zero-charge potential, wettability, ion adsorption, contact resistance and self-discharge characteristics. Many SFGs possess cation- and anion-exchange properties.[65]

Activated carbons can chemisorb molecular oxygen from the environment. On temperature rise, the chemisorption of oxygen increases; this gives rise to various functional groups on the carbon surface, *e.g.*, COOH, CO, quinone/hydroqiuonone and other groups. The oxygen-containing SFGs influence the stationary potential of AC electrodes; they also contribute to the main capacitance, and they can rapidly charge and discharge, which leads to increase in the Faradaic pseudocapacitance. An example of reversible redox reactions of SFGs that make a contribution to the Faradaic pseudocapacitance of AC electrodes is the oxidationj and reduction of the cyclic diacyl peroxide group (Scheme 1).

Scheme 1



Oxygen-[67] and nitrogen-containing[71] groups are encountered most often; sulfur- and boron-containing and other SFGs are also known.[72] Oxygen-containing groups are formed upon usual activation and upon the oxidation of carbon with oxygen or HNO_3 as well as electrochemical oxidation. The presence of oxygen has an adverse influence on the operation of SCs with non-aqueous electrolytes, since voltage instability appears, self-discharge accelerates and so on. Conversely, the capacitance of SCs with aqueous

electrolytes such as solutions of H_2SO_4 increases in the presence of oxygen-containing SFGs.

The results of measurements of galvanostatic curves with HDCM-based electrodes were used to establish the influence of redox reactions of SFGs on the energy efficiency of SCs.[16, 73] The energy efficiency of SCs, unlike that of batteries, is not limited by the polarization of electrode reactions, but is restricted only to the ohmic loss of energy; therefore, as noted above, the limiting efficiency of a double-layer SC may approach 100%. The energy densities for a symmetrical SC based on Norit activated carbon were calculated from the corresponding experimental galvanostatic curves. The experimental and theoretical dependences of the energy efficiency on the current for such SCs are presented in Fig. 6.[16] It can be seen that on moving towards higher currents, the efficiency first increases, reaches a maximum (~90%) and then decreases. This pattern of dependence is attributed to the fact that at low currents a considerable contribution to the total capacitance is made by the Faradaic (battery) process, which has a low energy efficiency due to polarization of the electrode reaction, whereas at high currents ohmic energy loss is manifested. In the case of medium currents, the capacitance is practically affected only by EDL (no pseudocapacitance processes or ohmic loss). Since the charge–discharge of EDL is reversible, its energy efficiency is maximized. Volfkovich *et al.*[16] developed a mathematical model that took into account both EDL charging and pseudocapacitance of the redox reactions of SFGs. The dependence of efficiency on the current calculated in this way was close to the experimental dependence (see Fig. 6), which confirms the accepted mechanism of SC operation.

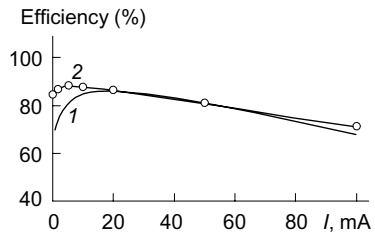


Figure 6. Calculated (*1*) and experimental (*2*) dependences of the efficiency on the current for SC based on Norit AC.[16] Published with permission from Springer.

As the current decreases, the capacitance increases (Fig. 7). In the region of large currents, the capacitance increases rather slowly, which is caused by decreasing ohmic losses. However, at low currents, the capacitance sharply increases up to 170 and 220 F g^{-1} during charging and discharging, respectively, because of the pronounced contribution of the pseudocapacitance of redox reactions of SFGs. A similar result was obtained in the study of the effect of redox reactions of SFGs for supercapacitors based on carbon black KJEC 600/Li in a non-aqueous electrolyte consisting of a 1 M solution of $LiPF_6$ in a mixture of ethylene carbonate (1/3), diethyl carbonate (1/3), and dimethyl carbonate (1/3).[73]

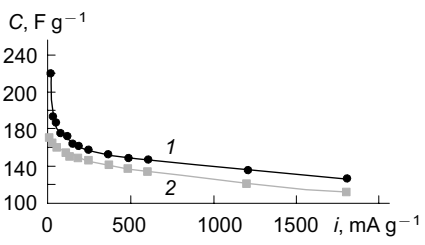


Figure 7. Dependences of the specific capacitance of SCs with Norit AC during charging (*1*) and discharging (*2*) on the current density.[16] Published with permission from Springer.

8. Porous structure and hydrophilic–hydrophobic properties of highly dispersed carbon electrodes

In some studies, the porous structure and hydrophilic–hydrophobic properties of electrodes based on HDCMs were studied by the standard contact porosimetry (SCP), which is recognized by IUPAC.[74–76] Unlike other methods including BET, this method makes it possible to study not only the porous structure of any material in a very broad range of pore radii (from ~1 to 3×10^5 nm), but also the hydrophilic–hydrophobic properties of materials. When octane is used as a measuring liquid, porosimetry curves are obtained for all pores, while the use of water gives porosimetry curves only for hydrophilic pores.

As noted above, HDCMs with a specific surface area of ~500 to 2500 m^2 g^{-1} are used as electrodes for supercapacitors. Carbon materials are known to have hydrophilic–hydrophobic properties, as they have both hydrophilic and hydrophobic pores.[74–76] Volfkovich *et al.*[32, 33] used the SCP method to study the CH900 active carbon cloth. The integral and differential curves for the specific pore volume *versus* pore size are shown in Fig. 8.[65] It can be used that the cloth has a very broad range of pores, extending from micropores with radii of $\leqslant$ 1 nm to macropores with radii of 1 to 100 μm, *i.e.*, the range of variation of the pore size is more than five orders of magnitude. This cloth has almost no mesopores with radii from 1 to 100 nm. The micropores ensure very high values of the total specific

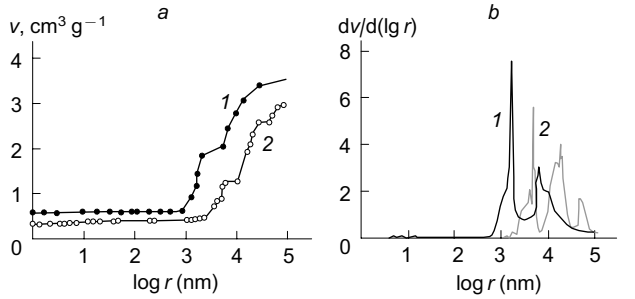


Figure 8. Integral (*a*) and differential (*b*) dependences on the specific pore volume (*v*) on the pore size (*r*) measured in octane (*1*) and in water (*2*) for the CH900 AC cloth.[65] Published with permission from Springer.

Table 1. Characteristics of the porous structure and hydrophilic–hydrophobic properties of various AC electrodes.[65]

Electrode	Specific surface area, m^2 g^{-1}		*II* : *I* ratio	Porosity, cm^3 cm^{-3}		
	I	*II*		*I*	*II*	*III*
CH900	1520	850	0.56	0.85	0.786	0.064
Viskumak	600	416	0.70	0.729	0.623	0.106
SAIT	940	520	0.55	0.715	0.490	0.225
Rikon	1705	825	0.48	0.762	0.673	0.089
KJEC900	2500	2600	—	0.89	0.84	0.05

Notes. The following designations for the specific surface area and porosity are used: *I* is total (against octane), *II* is hydrophilic (against water), *III* is hydrophobic.

surface area. The characteristics of the porous structure of some AC electrodes found using SCP are summarized in Table 1.

It can be seen that structure of all AC electrodes includes both hydrophilic and hydrophobic porosity. This is an important feature of carbon materials, which distinguishes them from purely hydrophilic (*e.g.*, metals, metal oxides and ion exchangers) or purely hydrophobic materials (*e.g.*, polytetrafluoroethylene, polyvinylidene fluoride and polyethylene). The hydrophilic–hydrophobic properties of AC should be taken into account when these carbons are used in SCs in aqueous electrolytes (electrochemical processes in these SCs take place only in hydrophilic pores). The total specific surface area of AC electrodes is relatively high ($600-2500\ m^2\ g^{-1}$) and may be considerably different. For different electrodes, the hydrophilic specific surface areas are also markedly different.

9. Study of the self-discharge of supercapacitors

9.1. Investigation methods

Most often, self-discharge is characterized by the time dependence of the open-circuit voltage of SCs after charging to a definite voltage, called the self-discharge profile.[77–95]

Typical self-discharge profiles for two SCs with and without electrode blocking layer are shown in Fig. 9. Both capacitors were potentiostatically charged up to 2.0 V for 18 h up to the open-circuit voltage.[77] The use of an ultrathin layer of electrodeposited poly(*p*-phenylene oxide) (PPO) as the blocking layer to decrease the leakage current, *i.e.*, self-discharge, was studied. The polymer was deposited on a glassy carbon electrode and, as can be seen from Fig. 9, the goal was attained: the self-discharge decreased.

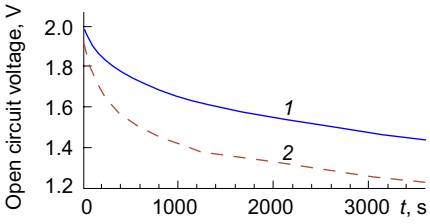


Figure 9. Self-discharge profiles in the supercapacitors with a blocking PPO layer (*1*) and without this layer (*2*). Both capacitors were charged to 2.0 V for 18 h to open circuit voltage.[77] Published with permission from Electrical and Electronics Engineers (IEEE).

Measurement of the leakage current. According to this method, a definite voltage is set on the terminals of a supercapacitor and the time variation of the current is recorded. Usually, after some (usually long) period of time, this descending curve reaches a plateau, which characterizes the leakage current. The greater the leakage current, the greater the self-discharge. The time variation of the normalized leakage currents at various voltages is illustrated by Fig. 10.

Kurzweil and Shamonin[96] carried out a comparative electrochemical study of SC with a neutral aqueous electrolyte, a 1 M solution of Li_2SO_4, and a liquid crystalline (LC) additive, 2% 4-n-pentyl-4′-cyanobiphenyl (5CB). It was shown that the capacitor containing an LC additive had a lower self-discharge and a lower leakage

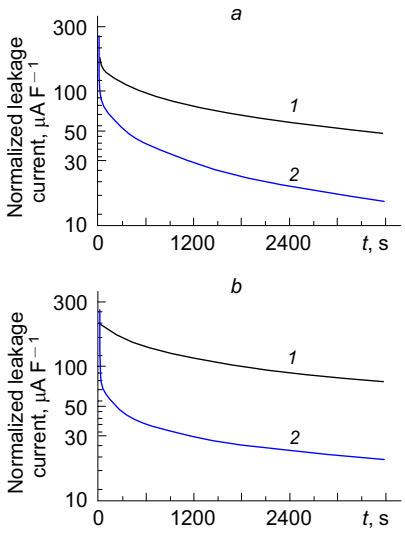


Figure 10. Time variation of the normalized leakage currents at voltages of 1 (*a*) and 1.2 V (*b*) for SCs with a neutral aqueous electrolyte (*1*) and with 2% 5CB additive (*2*).[95] Published with permission from MDPI.

current than the device containing no 5CB; furthermore, the addition of 5CB did not deteriorate the capacitance characteristics at various rated voltages. The effect is due to slower diffusion of ions hampering the self-discharge and a decrease in the leakage current, which is proportional to the Faradaic reaction. The rate of electron transfer depends on the redox reaction potential. According to the Tafel equation, the rate of the Faradaic reaction is exponentially related to the overvoltage, which results in an exponential increase in the leakage current with increasing applied voltage. In the ideal case, when the Faradaic reactions are completely absent, the leakage current is equal to zero; in this case, the measured capacitance is equal to the EDL capacitance.

Measurement of electrochemical impedance. This method was often used to study self-discharge.[77,97–103] The measured and calculated frequency dependences of the impedance for SCs with an ultrathin blocking layer of electrodeposited PPO (to decrease self-discharge) and the equivalent electrical circuit used in thie study are depicted in Fig. 11.[77] It can be seen that the impedance increases in the frequency range from 10^{-2} to 10^3 Hz in the presence of a blocking layer.

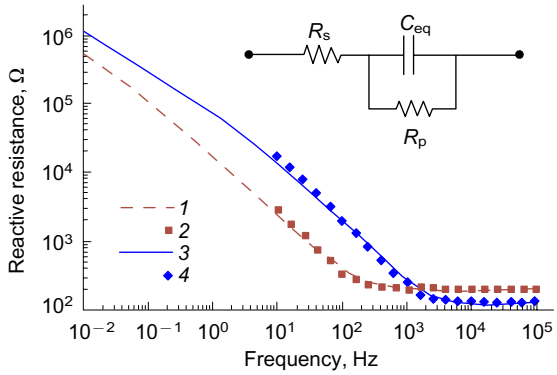


Figure 11. Measured (*1*, *3*) and calculated (*2*, *4*) frequency characteristics of impedance for SC with a blocking PPO layer (*3*, *4*) and without this layer (*1*, *2*) and equivalent electric circuit used for calculations.[77] C_{eq} is the EDL capacitance, R_s is series resistance, R_p is parallel resistance. Published with permission from Elsevier.

9.2. Self-discharge mechanisms

The following self-discharge mechanisms were established on the basis of studies of SCs based on carbon materials.

Redistribution of ions in a porous electrode across the thickness and among the pores of different sizes.[104, 105] In the case of long-term charging, ions are more uniformly distributed among different pores and across the thickness of electrodes; therefore, the oprn-circuit voltage decay after charging markedly decreases. The reported model can predict the effect of charging duration, initial voltage and temperature on the open-circuit voltage decay.[103–115] The charge redistribution is caused by different access of electrolyte ions to the inner surface of the electrode. At a higher initial voltage, SCs demonstrate a greater self-discharge, but at longer time of preliminary charge retention, the self-discharge rate becomes low. The restoration of the voltage was observed in SCs with graphene electrodes even after the complete discharge by the charge redistribution mechanism.[106]

Oxidation of carbon. It was shown[108, 109] that the key mechanisms of self-discharge in acidic aqueous electrolytes are the oxidation of carbon and charge redistribution. These processes are directed towards a decrease in the potential gradient in the electrodes. These processes are difficult to differentiate, as they are characterized by similar self-discharge profiles. A new experimental procedure was developed to solve this problem. It was found that the charge redistribution is the major mechanism of self-discharge in graphene electrodes, while the oxidation of carbon makes a lower, but still an important contribution (17% of the initial self-discharge).[106] A positive correlation between the self-discharge and the carbon oxidation rate was established. When the Spectracarb 2225 carbon cloth is used, carbon is oxidized to CO_2 and develops the surface functionality by forming C–O and C=O bonds. It is evident that at charging voltages, the positive electrode is predominantly oxidized, which leads to self-discharge acceleration. This can be seen in Fig. 12, which shows the dependences of voltage on time ($t^{1/2}$) for the SCA272 carbon capacitor with an organic electrolyte.[104]

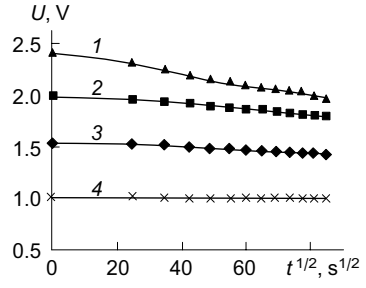


Figure 12. Dependences of the voltage on $t^{1/2}$ for the SCA272 capacitor over120 min of the self-discharge on the initial voltage: 2.4 (*1*), 2 (*2*), 1.55 (*3*) and 1 V (*4*).[104] Published with permission from Elsevier.

Initially, the C–O groups are mainly formed during charging of the electrode; the self-discharge gives mainly the C=O groups. The repeated charge–discharge cycles are accompanied by lower self-discharge, probably due to the depletion of the active sites of carbon oxidation. Hence, elimination of these active sites on the surface of the positive carbon electrode *via* electrochemical oxidation would significantly suppress the self-discharge in SCs with aqueous electrolytes.[108]

Shuttle self-discharge mechanism.[105, 108–113] A frequent case of shuttle self discharge is the migration of ions formed upon redox reactions from one electrode to the other associated with the presence of iron impurity in the electrolyte. As a result of electrically induced migration, Fe^{3+} ions get to the negative electrode where they are reduced to Fe^{2+}; after that, Fe^{2+} move to the positive electrode where they are oxidized again to Fe^{3+}, *etc*. The possible sources of iron in electrolyte solutions are ash or the products of corrosion of the supercapacitor casing. Conway[1] studied the effect of the shuttle migration of multicharged manganese and titanium ions on the self-discharge. Transition metal ions can be present not only as impurities in the electrolyte solution, but also as counter-ions of SFGs of active carbons. The shuttle migration of ions can be limited in several stages:[1, 104]

— polarization of electrode reactions, which depend on the catalyst activity;

— formation of a barrier in the form of EDL;

— diffusion and ohmic transport of ions between the electrodes.

It was shown[1, 29] that diffusion-controlled mechanism caused by the presence of impurities is implemented when $E > 1.4$ V for the positive electrode and when $E < 1.2$ V for the negative electrode.

According to Conway,[1] the self-discharge rates are described by the following relations:

— if the self-discharge is controlled by the diffusion of ions formed upon recharge or redox reactions of impurities, such as Fe^2/Fe^3 or other transition metal ions, the voltage decay would follow a linear dependence on time

$$U = U_1 - A\log(t + \theta), \tag{11}$$

where U_1 is the initial voltage, A is energy, t is time, θ is constant;

— in the case of self-discharge controlled by semi-infinite diffusion in a porous electrode (with impurities participating in a Faradaic process), the voltage decay is determined by the dependence of U on $t^{1/2}$

$$U_t = U_1 - \frac{2zFSD^{1/2}\pi^{1/2}ct^{1/2}}{c_0} \tag{12}$$

where U_t is the current voltage, z is the number of electrons, F is the Faraday number, S is the specific surface area of a porous electrode, D is the diffusion coefficient, c is the concentration of ions, c_0 is the initial concentration of ions;

— if the self-discharge is caused by the short-circuit leakage current between two electrodes, for example, due to faults in the assembly of an array of bipolar SCs, the dependence is linear

$$U_t = \ln U_1 - \frac{t}{RC} \tag{13}$$

where R is the ohmic resistance to leakage current.

The decrease in the voltage due to the self-discharge on a carbon cloth electrode with respect to the standard hydrogen electrode at various initial potentials in the 5.0 M H_2SO_4 electrolyte after charging with a 10 mA current is illustrated in Fig. 13. It can be seen that the $U(t)$ dependences are nearly linear, *i.e*., they obey Eqn (11).

Transport of ions from regions with high ion concentration to regions with lower ion concentration. It was found that self-discharge proceeds faster for SCs with carbon electrodes bearing many SFGs.[36, 105, 114–118] New methods for chemical modification of electrodes to retard the self-discharge caused by the presence of certain SFGs have

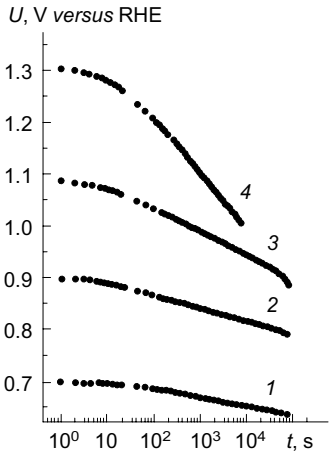


Figure 13. Voltage decay due to the self-discharge on the carbon cloth electrode at initial potentials of 0.7 (*1*), 0.9 (*2*), 1.1 (*3*), 1.3 (*4*) in the 5.0 M H_2SO_4 electrolyte after long-term charging with 10 mA current.[1]

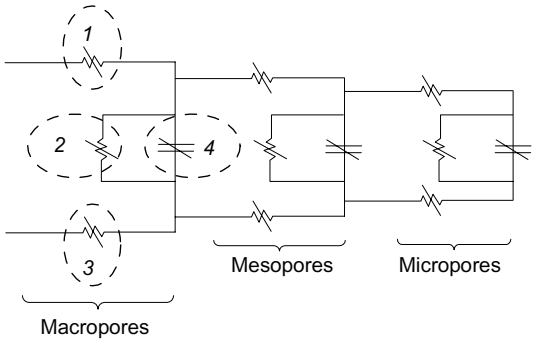


Figure 14. Equivalent electric circuit of the self-discharge in EDLC.[123] (*1*) electrolyte resistance, (*2*) resistance to self-discharge, (*3*) carbon resistance, (*4*) capacitance. Published with permission from Elsevier.

been considered.[36,119] Zhang *et al.*,[115] who studied self-discharge for SWCNT electrodes with a large number of SFGs, demonstrated that for the initial voltage of 1 V, self-discharge proceeds most rapidly in the first 30 min, while self-discharge to 0.5 V takes place within additional 4.15 h.

Yun *et al.*[118] considered the self-discharge of SCs with electrodes made of multi-walled carbon nanotubes of three different diameters — 20, 30 and 50 nm. The diffusion parameters found in terms of the developed model were in line with the measured self-discharge rates, which increase with increasing nanotube diameter. It was shown that the self-discharge processes depend on the pore size distribution and are closely related to the specific surface area of electrodes.

Elimination of the active surface sites on carbon positive electrodes by electrochemical cycling markedly reduces the self-discharge. This was demonstrated[107] in relation to supercapacitors with rGO electrodes.

The conclusions concerning the self-discharge mechanisms and, the more so, quantitative characteristics of self-discharge substantially depend on the electrode material; therefore, self-discharge has been studied for SC electrodes made of various carbon materials.[108,109]

9.3. Mathematical modelling of self-discharge

In a number of studies, the mathematical modelling of self-discharge was based on an adequate equivalent electric circuit. The electrochemical impedance method is very useful for studying the self-discharge of SCs.[79,89,120–123] The conventional equivalent circuits of capacitors have a basic series resistance (*RC* branch) and a parallel leakage resistance (R_p), which determines the self-discharge time.[89,120,122] Models of three parallel branches one of which contains a constant phase shift element have been considered.[78,123]

Kaus *et al.*,[123] who used A600 F Nesscap supercapacitors, found that self-discharge is determined by a number of parameters including the initial voltage, temperature and duration of charging. Depending on these parameters, a slight voltage decay (5–15%) was observed within 48 h after charging. A complex electrical model was developed to account for the redistribution effects of ions in supercapacitors. It was noted above that long-term charging leads to more uniform distribution of ions across the thickness of electrodes and among pores of various size; therefore, the open-circuit voltage decay after charging substantially decreases. The model is able to predict the effects of the duration of charging, the initial voltage and temperature on the open-circuit voltage decay. The equivalent circuit for self-discharge in EDLC, taking into account the resistance and capacitance of micro-, meso- and macropores, the electrolyte and carbon resistance and EDL capacitance, is depicted in Fig. 14.

The effect of duration of charging on the open-circuit voltage decay for charging durations of 15 min, 2 h and 5 days is shown in Fig. 15. When the charging durations were 2 h and 5 days, the voltage decays after 50 h were 6 and 3%, respectively. This is a very low self-discharge.[123]

An analytical approach to the modelling of self-discharge in SCs was developed by Tevi and Takshi.[124] A model comprising a system of equations that took into account charging of EDL, self-discharge equation and Tafel equation was developed. The experimental and calculated self-discharge profiles with and without the blocking layer are shown in Fig. 16. For decreasing the self-discharge, an electrodeposited ultrathin PPO blocking layer was used.

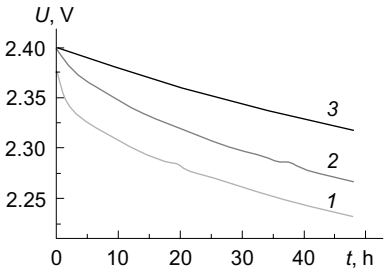


Figure 15. Effect of the duration of charging on the open circuit voltage decay with time. Duration of charging: 15 min (*1*), 2 h (*2*) and 5 days (*3*).[123] Published with permission from Elsevier.

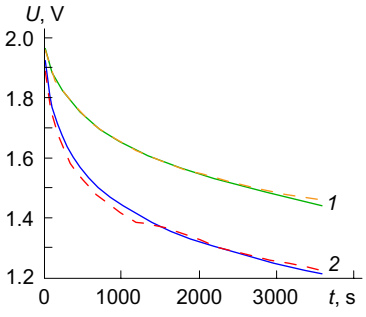


Figure 16. Experimental (continuous lines) and calculated (dashed lines) self-discharge profiles for SC with a blocking layer (*1*) and without this layer (*2*).[124] Published with permission from Elsevier.

Analysis of the presented data provides two conclusions:

— the blocking layer significantly reduces the self-discharge;

— the calculated profiles almost perfectly coincide with experimental data, which confirms the validity of the mathematical model to describe self-discharge.

10. Development of new supercapacitors with enhanced characteristics

10.1. Use of special additives to the electrolyte

Special additives to electrolytes are used in order to increase their viscosity, which increases the resistance and decreases self-discharge. Xia *et al.*[114] added the liquid crystals of 5CB to the electrolyte to suppress the self-discharge in EDLCs. If the capacitor is charged, the electrical field in EDL near the electrode surface induces the alignment of 5CB molecules; as this takes place, the viscosity of the liquid considerably increases due to the so-called electrorheological effect. Consequently, ion diffusion in the electrolyte can be hampered and the self-discharge rate decreases. For example, the addition of 2% 5CB reduced the open-circuit voltage decay rate and the leakage current in the $TEABF_4$–acetonitrile electrolyte by more than 80%. Haque *et al.*[125] introduced the liquid-crystalline 5CB additive into SC with an aqueous electrolyte, a 1 M solution of Li_2SO_4. The authors found that the 5CB-containing supercapacitor had a lower self-discharge and leakage current than the device without the additive, with no deterioration of the capacitance characteristics for various rated voltages. The effect of this additive on the self-discharge was attributed to the tunability of the effective conductivity of the composite electrolyte at the applied voltages, which leads to slower diffusion of ions and, hence, suppresses the self-discharge and leakage current.

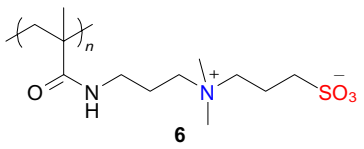
Liu *et al.*[126] used a lyotropic liquid crystal (LLC) as an electrolyte additive to suppress the self-discharge of SCs because of the electrorheological effect. The lyotropic liquid crystal formed by the Pluronic L64 triblock copolymer in the [Bmim]-BF_4 ionic liquid (1-butyl-3-methylimidazolium tetrafluoroborate) exhibited dielectric anisotropy and could reorient ions in an electric field, thus leading to enhanced viscosity and slower diffusion of ions in the electrolyte. It was shown that the addition of 5 vol.% LLC to the $TEABF_4$–acetonitrile electrolyte may reduce the self-discharge rate at room temperature by 32% with respect to SC containing no LLC. In view of the stability of LLC in a relatively broad temperature range, it is possible to reduce the self-discharge rate of a supercapacitor even at 50 °C.

An electrolyte additive based on 2-isocyanatoethyl methacrylate was polymerized on an AC electrode by two methods (electropolymerization *in situ* and radical polymerization) to reduce diffusion and self-discharge.[127] The radical polymerization demonstrated a considerable suppression of self-discharge; however, it also showed a sharp increase of all impedance parameters and deterioration of the charge – discharge characteristics. The electropolymerization method free from this drawback led to retention of the capacitance and suppressed the self-discharge.

10.2. Solid-state supercapacitors

Various types of solid-state supercapacitors are also used to minimize self-discharge. Ge and Liu[128] reported a solid-state SC with a zwitterionic gel electrolyte, which was prepared using compound **6**, poly[3-(3-(propylsulfonatedimethylammoniopropyl)methacrylamide]. This electrolyte provided a low self-discharge of solid-state SC during open circuit operation, while retaining the electrochemical characteristics during closed circuit operation.

Structure 6



6

Graphene-based electrodes have been used. A symmetric supercapacitor (SSC) was charged to 1.0 V at a constant current density of 100 μA cm^{-1} and then kept at this voltage for 4800 s to ensure full charging of the capacitor. After that, the open-circuit voltage decay was recorded. The self-discharge time down to half of the initial voltage was ~12 h for SSC based on compound **6**, which was almost twice longer than that for SSC based on polyvinyl alcohol (PVOH). It was noted that the zwitterionic gel electrolyte can be used to suppress the open-circuit diffusion of charged species, which is due to the decrease in the water activity caused by pronounced hydration of poly-zwitterions. The diffusion of charged species is suppressed due to their electrostatic interaction with the zwitterion groups. This is true for all zwitterionic gel electrolytes. The mechanism of the decrease in the self-discharge, described in detail in the cited publication,[128] can be extended to the zwitterionic gel electrolytes applied in other SCs and used to design a new strategy for meeting conflicting requirements of self-discharge minimization, while retaining electrochemical performance during closed-circuit operation of SCs.

Yu *et al.*[102] obtained a gel polymer electrolyte by adding methylene blue (MB) as a redox mediator into a mixture of poly(vinyl alcohol) and polyvinylpyrrolidone (PVP). The electrochemical performance of the quasi-solid-state SC with a gel polymer electrolyte (PVOH–PVP–H_2SO_4–MB) was evaluated by CV, galvanostatic charge–discharge, electrochemical impedance spectroscopy and self-discharge measurements. Upon the addition of MB, the specific capacitance of SC was 328 F g^{-1}, which is 164% higher than the specific capacitance of the supercapacitor with undoped electrolyte at the same current density (1 A g^{-1}). The energy density of SC increased from 3.2 to 10.3 W h kg^{-1}. The quasi-solid-state SC exhibited excellent cyclability over 2000 charge–discharge cycles.

Mishra *et al.*[129] considered electrochemical properties such as self-discharge and leakage current and discussed the voltage holding tests for solid-state symmetric SCs based on rGO, Whatman filter paper separator and gel electrolyte (PVOH – Na_2SO_4). Symmetric SCs showed a wide potential window (1.2 V), reasonably high specific capacitances (110.3 mA h g^{-1}) at a current density of 1 A g^{-1}, high energy density (22.1 W h kg^{-1}) and ultrahigh power density (7304.5 W kg^{-1}). Furthermore, these SCs showed 89.4% stability after 10 000 galvanostatic charge–discharge cycles, 82.3% capacitance after 20 h of self-discharge and also relatively low leakage current (0.029 mA).

Yun *et al.*[118] reported the design of solid-state flexible micro-supercapacitor (MSC) arrays with electrodes consisting of patterned multi-layer graphene, functionalized multi-layer carbon nanotubes and PVOH – H_3PO_4 gel electrolyte. The manufactured MSC showed areal capacitance of 2.54 mF cm^{-2} at a sweep rate of 10 mV s^{-2}; this capacitance was ~150 times higher than that of MSC with a

multi-layer graphene electrode. The areal energy and the power density were also considerably improved; in addition, there was no deterioration of the electrical performance after repeated convex and concave bending with a bending radius of 2.3 mm. Furthermore, it was possible to control the output voltage and the total capacitance of MSC by series or parallel connection of multiple planar-type MSCs, for example, in high-voltage light-emitting diodes. These MSCs showed reduced self-discharge.

10.3. Supercapacitors with ion exchange membranes

In recent years, studies were started on the application of ion exchange membranes (IEMs) in supercapacitors.[130–134] This is caused by the solid state of these SCs, which is convenient for practical use, and low self-discharge. Paleo *et al.*[130] reported solid-state hybrid supercapacitors with AC/MnO_2 electrodes deposited on a carbon nanofibre cotton fabric. These capacitors showed a stable performance in an aqueous medium for the voltage range of 0–1.6 V, low self-discharge and good capacitance performance of 138 and 134 F g^{-1} with porous paper and Nafion membrane, respectively. These values are in the same range as the values found in other related studies, but attained using simpler and cheaper materials (AC, carbon black, carbon nanofibres, dry MnO_2 powder). Solid-state HSC showed a very low self-discharge even after durability tests for 270 h. One more important conclusion of this study is demonstration of a stable operating voltage of 1.6 V, which is higher than the water splitting potential (1.23 V), without noticeable O_2 evolution or degradation of the electrodes.

The electrochemical performance of Nafion membranes was studied in solid-state SCs with rGO–Nafion membrane–CNTs–polypyrrole composites.[132] The Nafion 117 membranes were used as separators for a 1 M solution of LiCl as the electrolyte to fabricate solid-state symmetric SCs. The following characteristics were attained: specific capacitance of 258.3 F g^{-1} at a scan rate of 10 mV s^{-1} and the maximum energy and power densities of 10 W h g^{-1} and 6031 W kg^{-1}, respectively. The authors [132] fabricated a non-aqueous mechanically strong proton-conducting gel polymer electrolyte based on the 2-hydroxymethyl methacrylate monomer mixed with two solvents — propylene carbonate and *N*,*N*-dimethylformamide. The composite carbon electrode was manufactured by mixing the YP80-F and Kuraray active carbons with 5 mass % hexafluoropropylene as the binder. It was found that the capacitance performance varies depending on the gel electrolyte composition; at 20 °C, a specific capacitance of 90 F g^{-1} was attained. The electrochemical measurements were carried out over a broad temperature range from −40 to 80 °C.

The authors of most publications have studied SCs with proton exchange membranes, but some publications address SCs with anion exchange membranes. Li *et al.*[133] studied SCs in alkaline medium with OH^- conductivity in a polymer matrix. The authors revealed interesting relationships between the properties of polymer electrolyte and characteristics of the solid state SCs. The OH^--conducting polymer electrolytes were subdivided into two types: anion exchange membranes and alkaline polymer electrolytes. Capacitors with alkaline electrolytes usually have separators made of porous materials such as polypropylene, polyethylene or polyamide, which absorb the electrolyte, *i.e.*, act as insulators between the electrodes. Important properties of IEMs, which affect the SC performance, chemical stability and electrolyte absorption, were established. It was shown that reduced performance was due to evaporation of water; a way to suppress this effect was proposed. To fabricate a cost-effective, lightweight, thin and flexible solid-state SC with an anion exchange membrane, polymer electrolytes should have high ionic conductivity, a wide voltage window, the ability to form good electrode/electrolyte contacts, high mechanical strength (to withstand external loads) and chemical stability for long cycling.[134]

10.4. Use of electrolytes free from impurities

One of the key self-discharge mechanisms is the shuttle migration of ions (products of redox reactions) from one electrode to the other and back (see Section 9.2). A typical case of such shuttle self-discharge is the process caused by the presence of iron impurities in the electrolyte. The preparation of impurity-free electrolyte is highly important for the suppression of the self-discharge. It was noted above that the main source of impurities in the AC-based SC electrolyte is ash consisting of inorganic components; the main sources of ash are plant precursors: wood, nut shells, coconut hulls, *etc.* The ash is removed by dissolution in concentrated acids. One more way to prepare impurity-free electrolytes is to use carbide carbons as electrodes (see Section 6.3). A drastic solution to this problem is to use synthetic polymers such as polyethylene, polyacrylonitrile and so on as precursors.

The manufacturers of commercial SCs take adequate measures that virtually exclude the presence of impurities in electrolytes in order to minimize the self-discharge. For example, Shen *et al.*[135] measured the self-discharge for the commercial Maxwell BCAP 3000 supercapacitor with a rated capacitance of 3000 F and a rated voltage of 2.7 V at four temperatures (278, 293, 308 and 323 K) and five initial voltages (2.7, 2.4, 2.1, 1.8 and 1.5 V). The results of measurements of the self-discharge of this SC at various temperatures and initial voltages are shown in Fig. 17. It can be seen that at moderate temperatures (278, 293 and 308 K), the self-discharge was negligible over more than 100 000 s, but as the initial voltage and the temperature increased, the voltage decay at the terminals became more pronounced.

Similar results were obtained in another study.[83] A negligible self-discharge was also found [123] for commercial A600 F Nesscap supercapacitors (see Section 9.3, Fig. 14).

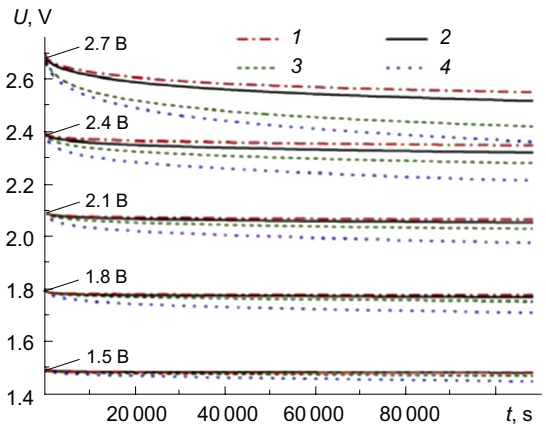


Figure 17. Self-discharge of the Maxwell BCAP 3000 SC at various temperatures and initial voltages.[135] *T*, K: (*1*) 278, (*2*) 293, (*3*) 308, (*4*) 323. Published with permission from Elsevier.

10.5. Methods of chemical modification of electrodes to suppress self-discharge

It was noted above that elimination of the surface active sites *via* electrochemical or chemical oxidation markedly suppresses the self-discharge of supercapacitors. It was found that the voltammetric cycling in a certain potential range leads to cleaning of the surface of rGO electrodes of supercapacitors from SFGs; this also markedly suppresses the self-discharge. It was also shown that this method is applicable to SCs with other HDCMs.

10.6. Hybrid supercapacitors

It was noted above that HSCs can be fabricated with different electrodes.[2,136–140] For example, one electrode is based om HDCM, and the other one is a battery electrode; alternatively, one electrode can be made of carbon, while the other one can be a PsC type electrode, in particular, based on electrically conductve polymers. The carbon electrode is often negative, because carbon can be oxidized at positive potentials. The main advantage of HSCs over EDLCs is the increase in the energy density, with the power density level being maintained, as a result of expansion of the potential window. The main drawback is decrease in the cyclability, which is limited by the non-polarizable electrode. As regards their characteristics, HSCs hold an intermediate position between EDLCs and batteries.

An example of HSC is the $^{+}(NiOOH \rightleftharpoons NiO_2)/KOH/C^{-}$ system in which a the positive electrode is a positive electrode of alkaline battery.[2] When AC is used as the base for the negative electrode, the range of variation of HSC potential is two times greater than that in EDLC and the energy density is 4–5 times higher. The maximum energy density of HSCs manufactured by the Russian company Esma is 11 W h kg^{-1}. The service life of this HSC is determined by the positive electrode, which is susceptible to degradation. For this HSC, 10 000 charge–discharge cycles were obtained.

Specialists of the CJSC Inkar and at the A.N.Frumkin Institute of Physical Chemistry and Electrochemistry, Russian Academy of Sciences (Russia), developed a new type of HSC with AC-based negative electrode, CH900 type cloth, and a $PbSO_4-H_2SO_4-PbO_2$ battery positive electrode.[2] The overall equation of reactions for this HSC has the form

$$PbO_2 + 2\,H_2SO_4 + (H^+)_{ads} \underset{-e^-}{\overset{e^-}{\rightleftarrows}} PbSO_4 + 2\,H_2O + (HSO_4^-)_{ads}$$

The maximum charging voltage (U_{max}) is ~2.1 V, and the minimum discharge voltage is 0.5 V. The minimum potential of the carbon electrode in the beginning of the discharge is −0.2 V, and the maximum potential at the end of the discharge is 1.0 V. Because if the Faradaic reaction of hydrogen intercalation into carbon during the deep cathodic charging, the limiting specific capacitance is 1110 F g^{-1}; therefore, the applied operation mode of this HSC also makes it possible to attain also high energy density. The indicated value U_{max} = 2.1 V, which is very high for aqueous electrolytes, is due to the high charging voltage of the $PbO_2/PbSO_4$ electrode equal to ~1.9 V. The specific energy finally attained for this HSC is 20–25 W h kg^{-1}, which is much higher than this value for symmetric carbon EDLCs. The service life of this HSC exceeds 10 000 charge–discharge cycles.

Kosova *et al.*[137] investigated the HSC based on mechanochemically activated samples of $LiCoPO_4$ cathodes and Kuraray K-50 AC anodes; a 1 M solution of $LiPF_6$ in an ethylene carbonate–dimethyl carbonate–ethyl methyl carbonate (1 : 1 : 1 v/v/v) was used as the electrolyte. A specific power of 1500 W kg^{-1} was attained for this HSC.

Hybrid supercapacitors of the PANI/AC type (PANI is polyaniline) were developed; SMK-3 activated carbon served as the negative electrode, while the PANI / SMK-3 was used as the positive electrode; and a 1 M solution of H_2SO_4 was used as the electrolyte. The energy density for these capacitors reached 23.8 W h kg^{-1}, with the power density being 206 W kg^{-1}.

Characteristics of some asymmetric and symmetric HSCs are summarized in Table 2.[10] It can be seen that asymmetric HSCs have higher energy density, but lower power density values.

Certain HSCs such as C/PbO_2, C/NiO_2, C/MnO_2 and C/ECPs have an enhanced specific energy (approximately 40–50 W h kg^{-1}); in this parameter, they are not inferior to some conventional batteries, but have much higher cyclability.[1,2]

Table 2. Characteristics of some HSCs based on ECPs.[10]

Electrodes	Operating voltage, V	Specific energy, W h kg^{-1}	Specific power, kW kg^{-1}
	Asymmetric HSCs		
$AC/LiMn_2O$	0.5–1.8	5–10	0.1–1
$Ni(OH)_2/AC$	0.5–1.7	2–10	0.08–2
AC/PbO_2	0–2	10–30	0.05–1
$AC/Li_4Ti_5O_{12}$	2–3	5–20	0.1–1
Graphite/AC	2–3.5	5–15	0.1–3
	Symmetric HSCs		
PANI/PANI	0–0.5	3.13	10–10.9
PPy/PPy	0–0.6	2.38	19–19.7
PEDOT/PEDOT	0–0.6	1.13	23–23.8
Carbon Maxorb/ Carbon Maxorb	0–0.7	3.74	22–22.4

Notes. The following designations are used: PPy is polypyrrole, PEDOT is poly(3,4-ethylenedioxythiophene), Carbon Maxorb is a carbon electrode manufactured by Maxorb.

10.7. Development of new supercapacitors

The development of new supercapacitors proceeds along a number of avenues that are listed below.

1. Design of highly dispersed carbon electrodes with a large specific surface area (~2000 m^2 g^{-1} and more). It is desirable that these S values be attained mainly due to mesopores, the greater fraction of which ensures enhanced characteristics at high charge and discharge rates. As an example, consider the study[141] reporting the fabrication of a new unique carbon material with S_{BET} = 3270 m^2 g^{-1}. The use of this material in SCs led to very high specific capacitance (870 F g^{-1}).

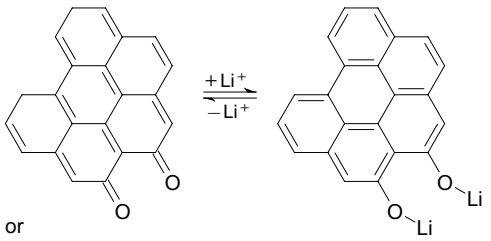
2. Development of new nanocomposites. Mohammadi *et al.*[61] fabricated new nanocomposites based on Co_3S_4 particles wrapped in CNT/rGO nanosheets. The rGO100-CNT50–Co_3S_4 electrode was chosen as the optimal one; it showed excellent electrochemical characteristics, in particular ultrahigh specific capacitance (977 F g^{-1} at a current density of 1 A g^{-1}) and a remarkable rate capability of 63% after the current density increased 40-fold. This

corresponded to the maximum energy density of 43.5 W h kg^{-1} and a power density of up to 6.9 kW kg^{-1}.

3. A very promising type of SCs are lithium cation exchange PsCs,[137, 142] which operate by a mechanism similar to the operation mechanism of lithium ion batteries (LIBs), but there are still considerable differences between them. Lithium ion batteries function on the basis of Faradaic reactions taking place in the bulk of the active material. This charge storage mechanism may provide a very high energy density (180 W h per 1 kg of the weight of LIB with graphene anodes) compared to conventional SCs. However, it is assumed that during charging lithium ions migrate from the inner part of the cathode active particle to the main part of the anode active particle, while during the discharge they migrate back. This implies intercalation–deintercalation processes taking place in both electrodes. Due to the very low rate of diffusion in the solid phase, these processes are kinetically controlled. As a result, LIBs show very low power density (100–1000 W kg^{-1}) and require a long time for recharging.

In modern PsCs with lithium ion exchange between the anode and the cathode, both electrodes are manufactured from materials based on highly porous graphene with a large specific surface area. A significant portion of the graphene surface is in contact with a liquid electrolyte, which ensures fast surface adsorption of lithium ions and/or interaction of SFGs; this eliminates the necessity of intercalation. Large surface area of the nanostructured anode facilitates fast deposition of a large amount of lithium ions; simultaneously, the electrochemical potential difference between the lithium-containing anode and cathode is restored. Graphene-based materials have definite surface functional groups (>C=O and >COOLi). As a result of charging and discharging, reversible redox reactions take place (Scheme 2).[136]

Scheme 2



$(>C{=}O)_{graphene} + Li^+ + e^- \rightleftharpoons (>C{-}OLi)_{graphene}$

Hence, these PsCs can be classified as redox supercapacitors. These lithium ion exchange cells can maintain a specific energy of 160 W h per kg of their weight, which is 30 times greater than this characteristic for conventional EDLCs. The specific power equal to 100 kW kg^{-1} is 10 times higher than that of conventional EDLCs and 100 higher than that of LIBs. Whereas for LIBs with a graphite anode and a $LiFePO_4$ cathode, a few hours are needed to complete the intercalation in one electrode and deintercalation in the other one, in the case of lithium ion exchange SCs, the time of ion migration is a few minutes. A wide range of these PsCs is associated with preliminary lithiation of the anode, which is solved using the third (lithium) electrode.

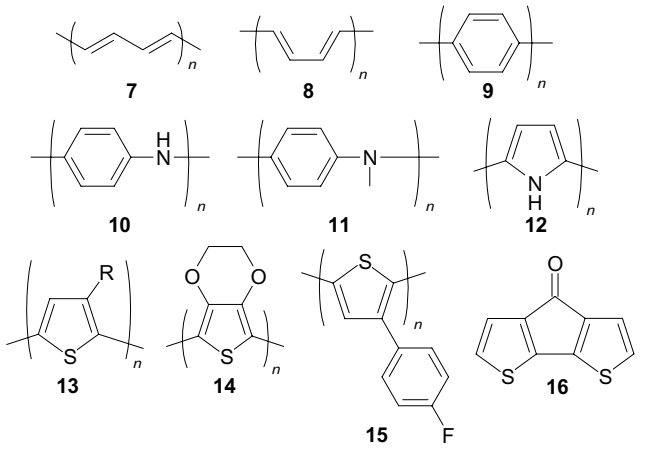
4. Use of metal nitrides (oxynitrides). In the fabrication of SCs, it is most important to design the electrode materials. Currently, metal nitrides (oxynitrides) have started to be used as electrodes in SCs, along with the widely used carbon or 2D materials, metal oxides (hydroxides) and materials based on conductive polymers. The theoretically estimated specific capacitance of these SCs is 1560 F g^{-1}. Nitride nanostructures showed excellent specific characteristics: the capacitance reached 990 F g^{-1}, the energy was up to 162 W h kg^{-1} and the power was up to 54 kW kg^{-1}.

A review by Ghosh *et al.*[143] focuses on recent achievements in the design of SCs based on nitrides (oxynitrides), including the mechanism of charge accumulation in them. The following nitrides were considered: Mo_2N/Co_3Mo_3N, Mo_3N_2 nanowires, TiN/CNTs, TiN/rGO, MnO_2-TiN/CNTs, $TiN-Li_4Ti_5O_{12}$/CNTs, PANI/TiN–CNTs, PPy/TiN/PANI–CNTs, VN, $Co(OH)_2$/VN, MnO_2–CNTs/VN–CNTs, Ni_3N/graphene, VO_xN_y, W(O,N), Ti(O,N).

5. Replacement of carbon atoms by nitrogen atoms in the crystal lattice of SCs. It was shown[144] that this new approach sharply increases the capacitance of SCs and increases the SC stability over charge–discharge cycles. By plasma treatment of carbon nanostructures, it is possible to replace 3% of carbon atoms in the crystal lattice by nitrogen atoms. The specific capacitance of nanowalls after such treatment reaches 600 F g^{-1}. This study demonstrates the possibility of manufacturing flexible thin-film SCs based on carbon nanowalls.

6. Design of electrodes based on ECPs. The development of electrically conductive polymers is an outstanding achievement of electrochemistry over the past 25 years. The electronic conduction of ECPs is implemented upon doping with counter-ions. In this case, delocalized π-electrons or holes are formed; under the action of an electric field, they migrate over the system of polyconjugated double bonds of polymer molecules. Conductive polymers are, for example, polyaniline, polyacetylene, polythiophene (PT), poly(*p*-phenylene), polypyrrole and their derivatives (structures **7**–**16**). Quasi-reversible electrochemical charge–discharge processes can take place in electrodes based on these polymers; therefore, these electrodes are widely used in SCs and are classified as PsC electrodes.[1, 2, 145–156]

Structures 7–16



Characteristics of some ECPs are summarized in Table 3. It can be seen that for some ECPs, the measured specific capacitances are higher than those for most carbon electrodes.

Characteristics of PsCs based on PDFPT and PcPT can be compared using data given in Table 4. For PsCs based

Table 3. Characteristics of ECPs used in pseudocapacitors.[145]

ECP	M_w, g mol^{-1}	Dopant level[a]	Potential range, V	Specific capacitance, F g^{-1}	
				calculated	experimental
PANI	93	0.5	0.7	750	240
PPy	67	0.33	0.8	620	530
PT	84	0.33	0.8	485	415
PEDOT	142	0.33	1.2	210	92

[a] Dopant level is the number of single-charged dopants (counter-ions) per monomer.

Table 4. Characteristics of some PsCs based on poly[3-(4-fluorophenyl)thiophene] (Poly-3), poly-3-(3,4-diflurophenyl)thiophene (PDFPT) and poly[3-(4-cyanophenyl)thiophene] (PcPT).[10]

Polymer	Cell voltage, V	Discharge time, s	Specific energy, W h kg^{-1}	Specific power, kW kg^{-1}
Poly-3	2.7	10	26.5	8
PDFPT	2.8	10	33	11
PcPT	2.9	10	45	11

on various ECPs, the specific energy is in the range from 26.5 to 45 W h kg^{-1}, while for EDLCs this range is markedly narrower: from 1 to 10 W h kg^{-1} (see Fig. 3).

Few studies address the self-discharge of PsCs with ECPs. Snook *et al.*[145] investigated the electrochemical characteristics of symmetric PsC based on C—Fe/PANI/Ni-GF (where Ni-GF is nickel graphene foam). This capacitor showed a very high maximum specific energy equal to 68.0 W h kg^{-1}, specific power of 718.2 W kg^{-1} at a current density of 1.0 A g^{-1} and a potential window of 0.0–1.7 V and also relatively low self-discharge (the voltage decreased from 1.3 to 0.9 V in 78 h).

Characteristics of commercially manufactured supercapacitors are presented in Table 5.[157–160] It can be seen that the highest specific power is inherent in SCs manufactured by ApowerCap, while the highest specific energy is characteristic of SCs manufactured by JSR Micro.

11. Conclusion

This review considers the main issues currently related to supercapacitors (SCs) all over the world. Despite the numerous advantages of SCs with carbon electrodes over batteries, described in this review, fast self-discharge is still a key drawback of supercapacitors. This problem was tackled by various groups of researchers who studied various types of highly dispersed carbon electrodes for SCs, effect of functional groups present in highly dispersed carbon materials, porous structure and hydrophilic–hydrophobic properties of such materials. The self-discharge phenomenon, the effect of carbon functional groups on the self-discharge and the mechanisms ofself-discharge were studied by a variety of methods and mathematical modelling of the self-discharge was performed.

The following approaches have been used in the world to minimize the main drawback of supercapacitors — fast self-discharge:

— use of certain electrolyte additives;

— design of solid-state supercapacitors;

— design of supercapacitors with ion exchange membranes;

— use of electrolytes without impurities,

— development of methods for chemical modification of electrodes.

Currently, supercapacitors with enhanced characteristics are being developed by the world community. New nanocomposites and highly dispersed carbon electrodes with a large specific surface area of about 2000 m^2 g^{-1} and more are being fabricated for this purpose; and highly promising lithium cation exchange pseudocapacitors and electrodes based on metal nitrides and oxynitrides are being designed.

Table 5. Characteristics of supercapacitors produced by various manufacturers.[10]

Manufacturer	U, V	R, mΩ	C, F	RC, s	Specific energy, W h kg^{-1}	Specific power, W kg^{-1}
Maxwell	2.7	0.375	2885	1.08	4.2	8836
	2.7	0.90	605	0.55	2.35	9597
ApowerCap	2.7	4.0	55	0.22	5.5	50 625
	2.7	1.4	450	0.58	5.89	24 595
Ness	2.7	0.55	1800	1.00	3.6	8674
	2.7	0.30	3640	1.10	4.2	8010
Carbon Tech	2.85	1.0	1600	1.6	5.8	9106
Asahi Glass	2.7	2.5	1375	3.4	4.9	3471
Panasonic	2.5	1.0	1200	1.2	2.3	4596
EPCOS	2.7	0.45	3400	1.5	4.3	6750
LS Cable	2.8	0.25	3200	0.80	3.7	12 400
BatScap	2.7	0.20	2680	0.54	4.2	18 225
Power Sys.	2.7	1.5	1350	2.0	4.9	5785
	3.3	3.0	1800	5.4	8.0	4320
Fuji Heavy	3.8	1.5	1000	2.6	9.2	10 375
JSR Micro	3.8	4.0	2000	4.0	12.1	9223

Note. The following designations are used: R is the resistance and C is the capacitance of SCs.

12. List of abbreviations and symbols

AC — activated carbon,
CNTs — carbon nanotubes,
CV — cyclic voltammetry,
ECPs — electron-conductive polymers,
EDLC — electrical double layer capacitor,
EDL — electrical double layer,
HDCM — highly dispersed carbon material,
HSC — hybrid supercapacitor,
IEM — ion exchange membrane,
LC — liquid crystal,
MSC — micro-supercapacitor,
PANI — polyaniline,
PPO — poly(*p*-phenylene oxide),
PVOH — poly(vinyl alcohol),
PVP — polyvinylpyrrolidone,
PsC — pseudocapacitor,
rGO — reduced graphene oxide,
SC — supercapacitor,
SCP — standard contact porosimetry;
SFGs — surface functional groups,
SSC — symmetrical supercapacitor,
SWCNTs — single-walled carbon nanotubes,
$TEABF_4$ — tetraethylammonium tetrafluoroborate,
A — discharge energy density,
C — capacitance,
C_g — specific capacitance per unit mass,
C_s — specific capacitance per unit area,
d — thickness of the capacitor plate,
D — diffusion coefficient,
E — potential,
EF — pulse efficiency,
i — discharge current density,
K — effective electrical conductivity of the electrolyte,
P_{ef} — discharge power,
P_{mi} — maximum power density,
P_{pi} — peak power density,
R — ohmic resistance to the leakage current,
S — specific surface area,
S_{BET} — Brunauer–Emmett–Teller specific surface area,
t — time,
U — voltage,
∋ — dielectric constant,
w — potential scan rate.

13. References

1. B.Conway. *Electrochemical Supercapacitors: Scientific Fundamentals and Technological Applications*. (Berlin: Springer, 2013)
2. V.S.Bagotsky, A.M.Skundin, Yu.M.Volfkovich. *Electrochemical Power Sources. Batteries, Fuel Cells, Supercapacitors*. (New York: Wiley, 2015)
3. Y.Li, Z.Pu, Q.Sun, N.Pan. *J. Energy Chem.*, **60**, 572 (2021)
4. A.Gopalakrishnan, S.Badhulika. *J. Power Sources*, **480**, 228830 (2020)
5. Y.Cao, S.Li, C.Xu, X.Ma, G. Huang, C.Lu, Z.Li. *ChemNanoMat.*, **7**, 1273 (2021)
6. G.Jiang, R.A.Senthil, Y.Sun, T.R.Kumar. *J. Power Sources*, **520**, 230886 (2022)
7. N.A.Rashidi, Y.H.Chai, I.S.Ismail, M.F.H.Othman. *Conver. Bioref.*, **20**, 55 (2022)
8. S.Rawat, R.K.Mishra, T.Bhaskar. *Chemosphere*, **286**, 131961 (2022)
9. M.E.Şahin, F.Blaabjerg, A.Sangwongwanich. *Energies*, **15**, 674 (2022)
10. Yu.M.Volfkovich. *Russ. J. Electrochem.*, **57**, 311 (2021)
11. S.Kumar, G.Saeed, L.Zhu, K.N.Hui, N.H.Kim, J.H.Lee. *Chem. Eng. J.*, **403**, 126352 (2021)
12. S.Saha, P.Samant, N.C.Murmua, T.Kuila. *J. Energy Storage*, **17**, 181 (2018)
13. Y.Zhang, S.Yu, G.Lou, Y.Shen, H.Chen, Z.Shen, S.Zhao, J.Zhang, S.Chai, Q.Zou. *J. Mater. Sci.*, **52**, 11201 (2017)
14. N.S.Lidorenko. *Dokl. Akad. Nauk SSSR*, **216**, 1261 (1974)
15. Yu.M.Volfkovich, A.N.Filippov, V.S.Bagotsky. *Structural Properties of Porous Materials and Powders Used in Different Fields of Science and Technology*. (London; Springer, 2014)
16. Yu.M.Volfkovich, D.A.Bograchev, A.Yu.Rychagov, V.E.Sosenkin, M.Yu.Chaika. *J. Solid State Electrochem.*, **19**, 1 (2015)
17. Y.Oren. *Desalination*, **228**, 10 (2008)
18. Yu.M.Volfkovich. *Russ. J. Electrochem.*, **56**, 18 (2020)
19. Yu.M.Volfkovich, T.M.Serdyuk. *Russ. J. Electrochem.*, **38**, 935 (2002)
20. K.Fic, M.Meller, J.Menzel, E.Frackowiak. *Electrochim. Acta*, **206**, 496 (2016)
21. J.Kowal, E.Avaroglu, F.Chamekh, A.Šenfelds. *J. Power Sources*, **196**, 573 (2011)
22. P.Venet, Z.Ding, G.Rojat, H.Gualous. *Eur. Power Electron. Drives*, **17**, 6 (2007)
23. J.R.Miller. *J. Power Sources*, **326**, 726 (2016)
24. I.G.Gurevich, Volfkovich, V.S.Bagotskii. *Zhidkostnye Poristue Electrody. (Liquid Porous Electrodes)*. (Minsk: Nauka i Technika, 1974)
25. Yu.M.Volfkovich, V.M.Mazin, N.A.Urisson. *Russ. J. Electrochem.*, **34**, 740 (1998)
26. M.Inagaki, H.Konno, O.Tanaike. *J. Power Sources*, **195**, 7880 (2010)
27. A.Yu.Rychagov, M.Yu.Izmailova, V.E.Sosenkin, Yu.M.Volfkovich, K.K.Denshxhikov. *Electrochem. Energet.*, **15**, 3 (2015)
28. Y.Lu, S.Zhang, J.Yin, C.Bai, J.Zhang, Y.Li, Y.Yang, Z.Ge, M.Zhang, L.Wei, M.Ma, Y.Ma, Y.Chen. *Carbon*, **124**, 64 (2017)
29. M.N.Efimov, V.E.Sosenkin, Yu.M.Volfkovich, A.A.Vasilev, D.G.Muratov, S.A.Baskakov, O.N.Efimov, G.P.Karpacheva. *Electrochem. Commun.*, **96**, 98 (2018)
30. A.Borenstein, O.Hanna, R.Attias, S.Lusk. *J. Mater. Chem. A*, **5**, 12653 (2017)
31. H.Wang, Y.Zhong, Q.Li, J.Yang, Q.Dai. *J. Phys. Chem. Solids*, **69**, 2420 (2008)
32. Yu.M.Volfkovich, A.A.Mikhailin, D.A.Bograchev, V.E.Sosenkin, V.S.Bagotsky. *Recent Trend Electrochem. Sci. Technol.*, 159 (2012)
33. Yu.M.Volfkovich, D.A.Bograchev, A.A.Mikhalin, V.S.Bagotsky. *J. Solid State Electrochem.*, **18**, 1351 (2014)
34. H.Nishihara, H.Itoi, T.Kogure, P.Hou, H.Touhara, F.Okino, T.Kyotani. *Chem.–Eur. J.*, **15**, 5355 (2009)
35. A.V.Rychagov, Yu.M.Volfkovich, M.A.Vorotyntsev, L.D.Kvacheva, D.V.Konev, A.V.Krestinin, Yu.G.Kryazhev, V.L.Kuznetsov, Yu.A.Kukushkina, V.M.Mukhin, V.V.Sokolov, S.P.Chervonobrodov. *Electrochem. Energet.*, **12**, 167 (2012)
36. T.Ariyanto, J.Glaesel, A.Kern, G.Zhang, B.J.Etzold. *Beilstein J. Nanotechnol.*, **10**, 419 (2019)
37. B.Krüner, C.Odenwald, A.Tolosa, A.Schreiber, M.Aslan, G.Kickelbick, V.Presser. *Sustain. Energy Fuels*, **1**, 1588 (2017)
38. X.Yang, B.Fei, J.Ma, L.Liu, X.Liu, S.Yang, G.Tian, Z.Jiang, S.Yang, G.Tian, Z.Jiang. *Carbohydr. Polym.*, **180**, 385 (2018)
39. Yu.M.Volfkovich, V.E.Sosenkin, N.A.Maiorova, A.Yu.Rychagov, S.A.Baskakov, E.N.Kabachkov, V.I.Korepanov, N.N.Dremova, Yu.V.Baskakova, Yu.M.Shul'ga. *Colloid J.*, **83**, 284 (2021)

40. Yu. M.Volfkovich, A.Yu.Rychagov, V.E.Sosenkin, A.V.Krestinin. *Electrochem. Energet*., **8**, 106 **(**2008)
41. Z.Yang, J.Tian, Z.Yin, C.Cui, W.Qian, F.Wei. *Carbon*, **141**, 467 (2019)
42. Yu.M.Volfkovich, A.Yu.Rychagov, V.E.Sosenkin, O.N.Efimov, M.I.Os'makov, A.F.Seliverstov. *Russ. J. Electrochem*., **50**, 1099 (2014)
43. B.Dong, B.-L.He, C.-L.Xu, H.-L.Li. *Mater. Sci. Eng. B*, **143**, 7 (2007)
44. J.Wang, Y.Xu, X.Chen, X.Sun. *Compos. Sci. Technol*., **67**, 2981 (2007)
45. F.Li, J.Qu, J.Wang, V.Bandari, F.Zhu, O.Schmidt. *Nano Mater. Sci*., **3**, 154 (2021)
46. Y.Honda, M.Takeshige, H.Shiozaki, T.Kitamura, K.Yoshikawa, S.Chakarabarti, O.Suekane, L.Pan, Y.Nakayama, M.Yamagata, M.Ishikawa. *J. Power Sources*, **185**, 1580 (2008)
47. W.K.Chee, W.K Lim, H.N.Zainal, Z.Huang, N.M.Harrison, Y.Andou. *J. Phys. Chem. C*, **120**, 4153 (2016)
48. A.Eftekhari, Yu.M.Shulga, S.A.Baskakov, G.L.Gutsev. *Int. J. Hydrogen Energy*, **43**, 2307 (2018)
49. Yu.M.Shulga, S.A.Baskakova, Yu.V.Baskakova, A.S.Lobach, E.N.Kabachkov, Yu.M.Volfkovich, V.E.Sosenkin, N.Yu.Shulga, S.I.Nefedkin, Y.Kumar, A.Michtchenko. *J. Alloys Compd.*, **730**, 88 (2018)
50. Yu.M.Shulga, S.A.Baskakov, Yu.V.Baskakova, A.S.Lobach, Yu.M.Volfkovich, V.E.Sosenkin, N.Yu.Shulga, Y.N.Parkhomenko, A.Michtchenko, Y.Kumar. *Microporous Mesoporous Mater*., **245**, 24 **(**2017)
51. Yu.G.Kryazhev, Yu.M.Volfkovich, V.P.Mel'nikov, A.Yu.Rychagov, M.V.Trenikhin, V.S.Solodovnichenko, V.A.Likholobov. *Prot. Metals Phys. Chem. Surfaces*, **53**, 422 (2017)
52. Yu.M.Shulga, S.A.Baskakov, Yu.V.Baskakova, Yu.M.Volfkovich, N.Yu.Shulga, E.A.Skryleva, Y.N.YParkhomenko, K.G.Belay, G.L.Gutsev, A.Yu.Rychagov, V.E Sosenkin, I.D.Kovalev. *J. Power Sources*, **279**, 722 (2015)
53. Q.Ke, J.Wang. *J. Materiomics*, **2**, 37 (2016)
54. Patent US 10214422 B2 (2019)
55. X.Yang, C.Cheng, Y.Wang, L.Qiu, D.Li. *Science*, **341**, 534 (2013)
56. H.Liu, Y.Wang, X.Gou, T.Qi, J.Yang, Y.Ding. *Mater. Sci. Eng. B*, **178**, 293 **(**2013)
57. H.Aboutalebi, A.T.Chidembo, M.Salari, K.Konstantinov, D.Wexler, H.K.Liu, S.X.Dou. *Energy Environ. Sci*., **4**, 1855 **(**2011)
58. M.Zhong, Y.Song, Y.Li, C.Ma, X.Zhai, J.Shi, Q.Guo, L.Liu. *J. Power Sources*, **217**, 6 (2012)
59. D.Sun, X.Yan, J.Lang, Q.Xue. *J. Power Sources*, **222**, 52 (2013)
60. Z.Zhou, X.F.Wu. *J. Power Sources*, **222**, 410 (2013)
61. A.Mohammadi, N.Arsalani, A.G.Tabrizi, S.E.Moosavifard, Z.Naqshbandi, L.S.Ghadimi. *Chem. Eng. J*., **334**, 66 (2018)
62. V.A.Smirnov, N.N.Denisov, N.N.Dremova, Yu.M.Volfkovich, A.Yu.Rychagov, V.E.Sosenkin, K.G.Belay, G.L.Gutsev, N.Yu, Yu.M.Shulga. *Appl. Phys. A*, **117**, 1859 (2014)
63. Yu.M.Volfkovich, A.S.Lobach, N.G.Spitsyna, S.A.Baskakov, V.E.Sosenkin, A.Yu.Rychagov, E.N.Kabachkov, A.Sakars, A.Michtchenko, Yu.M.Shulga. *J. Porous Mater*., **26**, 1111 (2019)
64. W.Yu, L.Sisi, Y.Haiyan, L.Jie. *RSC Adv*., **10**, 15328 (2020)
65. Yu.M.Volfkovich, A.A.Mikhalin, A.Yu.Rychagov, V.E.Sosenkin, D.A.Bograchev. *Russ. J. Electrochem*., **56**, 869 (2020)
66. M.P.Tarasevich. *Elektrokhimiya Uglerodnykh Materialov. (Electrochemistry of Carbon Materials)*. (Moscow: Nauka, 1984)
67. I.A.Tarkovskaya. *(Okislennyi Ugol'). (Oxidized Coal)*. (Kiev: Naukova Dumka, 1981)
68. A.S.Ermakova, A.V.Popova, M.Yu.Chayka, T.A.Kravchenko. *Russ. J. Electrochem*., **53**, 608 (2017)
69. A.S.Solyanikova, M.Yu.Chayka, V.A.Parfenov, S.D.Kirik, T.A.Kravchenko. *Russ. J. Electrochem*, **51**, 764 (2015)
70. Yu.M.Volfkovich, I.V.Goroncharovskaya, A.K.Evseev, V.E.Sosenkin, M.M.Gol'din. *Russ. J. Electrochem*., **53**, 1367 (2017)
71. E.Frackowiak, G.Lota, J.Machnikowski, C.Vix-Guterl, F.Béguin. *Electrochim. Acta*, **51**, 2209 (2006)
72. S.Sepehri, B.B.Garcia, Q.Zhang, G.Cao. *Carbon*, **47**, 1436 (2009)
73. D.A.Bograchev, D.Yu.Gryzlov, V.E.Sosenkin, Yu.M.Volfkovich. *Electrochim. Acta*, **319**, 522 (2019)
74. Yu.M.Volfkovich, A.V.Sakars, A.A.Volinsky. *Int. J. Nanotechnol*., **2**, 292 (2005)
75. Yu.M.Volfkovich, V.E.Sosenkin. *Russ. Chem. Rev*., **81**, 939 (2012)
76. J.Rouquerol, G.Baron, R.Denoyel, H.Giesche, J.Groen, P.Lobes, P.Levitz, A.V.Neimark, S.Rigby, R.Skudas, K.Sing, M.Thommes, K.Unger. *Pure Appl. Chem*., **84**, 107 **(**2012)
77. T.Tevi, H.Yaghoubi, J.Wang, A.Takshi. *J. Power Sources*, **241**, 586 (2013)
78. Y.Diab, P.Venet, H.Gualous, G.Rojat. *IEEE Transact. Power Electronics*, **24**, 510 (2008)
79. C.Hao, X.Wang, Y.Yin, Z.You. *J. Electron. Mater*., **45**, 2161 (2016)
80. B.E.Conway, W.G.Pell, T.-C.Liu. *J. Power Sources*, **65**, 53 (1997)
81. J.Zhao, A.F.Burke. *J. Energy Chem*., **59**, 276 (2021)
82. P.Saha, K.Roy, P.Nambisan. In *International Conference on Signal Processing, Communication, Power and Embedded System (SCOPES)-2016*. Odisha, India, 2016; https://doi.org/10.1109/TENCON.2019.8929684 (Last access 15.06.2022)
83. L.I.Zhongxue, W.Fu. In *IEEE 2011 Asia-Pacific Power and Energy Engineering Conference (APPEEC)*; https://doi.org/10.1109/APPEEC.2011.5748403 (Last access 15.06.2022)
84. C.Zhao, X.Sun, W.Li, M.Shi, K.Ren, X.Lu. *ACS Appl. Energy Mater*., **4**, 8070 (2021)
85. Q.Abbas, F.Béguin. *Prog. Nat. Sci.: Mater. Int*., **25**, 622 (2015)
86. V.R.S.Visentini, L.M.C.Zarpelon, R.N.Faria Jr. *Mater. Sci. Forum*, **802**, 427 (2014)
87. M.R.Jisha, Y.J.Hwang, J.S.Shin, K.S.Nahm, T.P.Kumar, K.Karthikeyan, N.Dhanikaivelu, D.Kalpana, N.G.Renganathan, A.M.Stephan. *Mater. Chem. Phys*., **115**, 33 (2009)
88. T.J.Freeborn, A.Allagui, A.Elwakil. In *2017 European Conference on Circuit Theory and Design (ECCTD)*. Catania, Italy, 2017; https://doi.org/10.1109/ECCTD.2017.8093337 (Last access 15.06.2022)
89. F.Yu, M.Huang, J.Wu, Z.Qiu, L.Fan, J.Lin, Y.Lin. *J. Appl. Polym. Sci*., **131**, 39784 (2014)
90. S.Dsoke, Q.Abbas. *ChemElectroChem*., **7**, 2466 (2020)
91. N.Wu, X.Bai, D.Pan, B.Dong, R.Wei, N.Naik, R.R.Patil, Z.Guo. *Adv. Mater. Interfaces*, **8**, 2001710 (2021)
92. H.Miniguano, A.Barrado, C.Fernández, P.Zumel. *Energies*, **12**, 1776 (2019)
93. Z.Li, S.He, C.Ji, H.Mi, C.Lei, Z.Li, H.Pang, Z.Fan, C.Yu, J.Qiu. *Adv. Mater. Interfaces*, **6**, 1900959 (2019)
94. J.Gonzalez-Llorente, A.A.Lidtke, K.Hatanaka, L.Lakhdar, I.Fajardo, K.I.Okuyama. *Acta Astronaut*., **174**, 294 (2020)
95. K.Liu, C.Yu, W.Guo, L.Ni, J.Yu, Y.Xie, Z.Wang. *J. Energy*, **58**, 94 (2021)
96. P.Kurzweil, M.Shamonin. *Batteries*, **4**, 35 (2018)
97. J.F.Shen, Y.J.He, Z.F.Ma. *J. Power Sources*, **303**, 294 (2016)

98. P.Saha, M.Khanra. In *International Conference on Signal Processing, Communication, Power and Embedded System (SCOPES)-2016*. Odisha, India, 2016; https://doi.org/10.1109/SCOPES.2016.7955667 (Last access 15.06.2022)
99. H.E.Brouji, J.M.Vinassa, O.Briat. In *IEEE Vehicle Power and Propulsion Conference*. Harbin, China; https://doi.org/10.1109/VPPC.2008.4677493 (Last access 15.06.2022)
100. M.O.Bamgbopa, D.Belaineh, D.A.Mengistie, J.Edberg, I.Engquist, M.Berggren, K.Tybrandt. *J. Mater.Chem. A*, **9**, 2184 (2021)
101. N.Rizoug, P.Bartholomeus. *IEEE Transact. Indust. Electron.*, **57**, 3980 (2010)
102. F.Yu, M.Huang, J.Wu, Z.Qiu, L.Fan, J.Lin, Y.Lin. *J. Appl. Polym. Sci.*, **131**, 39784 (2014)
103. H.Wang, Q.Zhou, B.Yao, H.Ma. *Adv. Mater. Interfaces*, **5**, 1701547 (2018)
104. B.W.Ricketts, C.Ton-That. *J. Power Sources*, **89**, 64 (2000)
105. M.Ceraolo, G.Lutzemberger, D.Poli. *J. Energy Storage*, **11**, 211 (2017)
106. H.Yang, Y.Zhang. *J. Power Sources*, **196**, 8173 (2011)
107. M.A Davis, H.A.Andreas. *Carbon*, **139**, 299 (2018)
108. A.M.Oickle, J.Tom, H.A.Andreas. *Carbon*, **110**, 232 (2016)
109. O.Okhay, A.Tkach, P.Staiti, F.Lufrano. *Electrochim. Acta*, **353**, 136540 (2020)
110. H.A.Andreas, J.M.Black, A.A.Oickle. *Electrochim. Acta*, **140**, 116 (2014)
111. T.Yumak, D.Bragg, E.M.Sabolsky. *Appl. Surface Sci.*, **469**, 983 (2019)
112. F.Rafik, H.Gualous, R.Gallay, A.Crausaz. *J. Power Sources*, **165**, 928 (2007)
113. S.A.Kazaryan, S.V.Litvinenko, G.G.Kharisov. *J. Electrochem. Soc.*, **155**, A464 (2008)
114. M.Xia, J.Nie, Z.Zhang, X.Lu, Z.L.Wang. *J. Power Sources*, **47**, 43 (2018)
115. Q.Zhang, C.Cai, J.Qin, B.Wei. *Nano Energy*, **4**, 14 (2014)
116. H.Miniguano, A.Barrado, C.Fernández, P.Zumel, A.Lázaro. *Energies*, **12**, 1 (2019)
117. S.Subramanian, M.A.Johny, M.M.Neelanchery, S.Ansari. *IEEE Trans. Power Electron.*, **33**, 10410 (2018)
118. J.Yun, D.Kim, G.Lee, J.S.Ha. *Carbon*, **79**, 156 (2014).
119. S.Satpathy, M.Dhar, B.K.Bhattacharyya. *J. Energy Storage*, **31**, 101606 (2020)
120. A.Schneuwly, R.Gallay. *Proc. PCIM*, **2**, 1 (2000)
121. T.Ghanbari, E.Moshksar, S.Hamedi, F.Rezaei, Z Hosseini. *J. Power Sources*, **495**, 229787 (2021)
122. V.Musolino, L.Piegari, E.Tironi. *J. Mag. IEEE Transact. Ind. Electron.*, **60**, 112 (2012).
123. M.Kaus, J.Kowal, D.U.Sauer. *Electrochim. Acta*, **55**, 7516 (2010)
124. T.Tevi, A.Takshi. *J. Power Sources*, **273**, 857 (2015)
125. M.Haque, Q.Li, A.D.Smith, V.Kuzmenko. *J. Power Sources*, **453**, 227897 (2020)
126. M.Liu, M.Xia, R.Qi, Q.Ma, M.Zhao, Z.Zhang. *ChemElectroChem*, **6**, 2531 (2019)
127. J.Chung, H.Park, C.Jung. *Electrochim. Acta*, **369**, 137698 (2021)
128. K.Ge, G.Liu. *Chem. Commun.*, **55**, 7167 (2019)
129. R.K.Mishra, G.J.Choi, Y.Sohn, S.H.Lee, J.S.Gwag. *Mater. Lett.*, **253**, 250 (2019)
130. A.J.Paleo, P.Stait, A.Brigandì, F.N.Ferreira, A.M.Rocha, F.Lufrano. *Energy Storage Mater.*, **12**, 204 (2018)
131. M.G.Hosseini, H.Rasouli, E.Shahryari, L.Naji. *J. Appl. Polym. Sci.*, **13**, 44926 (2017).
132. A.A.Łatoszyńska, P.Taberna, P.Simon, W.Wieczorek. *Electrochim. Acta*, **242**, 31 (2017)
133. J.Li, J.Qiao, K.Lian. *Energy Storage Mater.*, **24**, 6 (2020)
134. K.Liu, C.Yu, W.Guo, L.Ni, J.Yu, Y.Xie, Z.Wang. *J. Energy. Chem.*, **58**, 94 (2021)
135. J.F.Shen, Y.J.He, Z.F.Ma. *J. Power Sources*, **303**, 294 (2016)
136. Z.Li, S.Wang, X.Liu, L.S.Yang. *J. Power Sources*, **196**, 8160 **(**2011)
137. N.V.Kosova, T.L.Kulova, N.F.Nikolskaya, O.A.Podgornova, A.Yu.Rychagov, V.E.Sosenkin, Yu.M.Volfkovich. *J. Solid State Electrochem.*, **23**, 1981 (2019)
138. M.K.Singh, S.A.Hashmi. *Ionics*, **23**, 1 (2017)
139. R.Genc, M.O.Alas, E.Harputlu, S.Repp, N.Kremer, M.Castellano, S.G.Colak, K.Ocakoglu, E.Erdem. *Sci. Rep.*, **7**, 1 (2017)
140. X.Gao, L.Zu, X.Cai, C.Li, H.Lian, Y.Liu, X.Wang, X.Cui. *Nanomaterials*, **8**, 335 (2018)
141. Yu.M.Volfkovich, V.E.Sosenkin, A.Yu.Rychagov, A.V.Melezhik, A.G.Tkachev, E.N.Kabachkov, V.I.Korepanov, I.I.Khodos, A.Michtchenko, Yu.M.Shulga. *Microporous Mesoporous Mater.*, **319**, 111063 (2021)
142. B.Z.Jang, C.Liu, D.Neff, Z.Yu, M.C.Wang, W.Xiong, R.Zhamu. *Nano Lett.*, **11**, 3785 (2011)
143. S.Ghosh, S.M.Jeong, S.R.Polaki. *Korean J. Chem. Eng.*, **35**, 1389 (2018)
144. S.A.Evlashin, Y.M.Maksimov, P.V.Dyakonov, A.A.Pilevsky, K.I.Maslakov, Y.A.Mankelevich, E.N.Voronina, S.V.Vavilov, A.A.Pavlov, E.V.Zenova, I.S.Akhatov, N.V.Suetin. *Sci. Rep.*, **9**, 6716 (2019)
145. G.A.Snook, P.Kao, A.S.Best. *J. Power Sources*, **196**, 1 (2011)
146. C.Peng, S.Zhang, D.Jewell, G.Z.Chen. *Prog. Nat. Sci.*, **8**, 777 (2008)
147. Z.Huang, L.Li, Y.Wang, C.Zhang, T.Liu. *Compos. Commun.*, **8**, 83 (2018)
148. J.Wang, Y.Xu, X.Chen, X.Sun. *Compos. Sci. Technol.*, **67**, 2981 2007
149. B.C.Kim, J.S.Kwon, J.M.Ko, J.H.Park, C.O.Too, G.G.Wallace. *Synth. Met.*, **160**, 94 (2010)
150. H.P.Cong, X.C.Ren, P.Wang, S.H.Yu. *Energy Environ. Sci.*, **6**, 1185 (2013)
151. M.Ates, A.S.Sarac. *Polym.-Plast. Technol. Eng.*, **50**, 1130 (2011)
152. J.J.Cai, L.B.Kong, J.Zhang, Y.C.Luo, L.Kang. *Chin. Chem. Lett.*, **21**, 1509 (2010)
153. M.Yang, B.Cheng, H.Song, X.Chen. *Electrochim. Acta*, **55**, 7021 **(**2010)
154. Y.Fang, J.Liu, D.J.Yu, J.P.Wicksted, K.Kalkan, C.Q.Topal, B.N.Flanders, J.Wu, J.Li. *J. Power Sources*, **195**, 674 (2010)
155. M.A.Vorotyntsev, D.V.Konev, C.H.Devillers, I.Bezverkhyy, O.Heintz. *Electrochim. Acta*, **56**, 3436 (2011)
156. M.N.Rantho, M.J.Madito, N.Manyala. *J. Alloys Compd.*, **819**, 52993 (2020)
157. A.Burke, M.Mille. *J. Power Sources*, **196**, 514 (2011)
158. J.R.Miller. *Appl Surface Sci.*, **460**, 3 (2018)
159. M.Yassine, D.Fabris. *Energies*, **10**, 1340 (2017)
160. L.Zhang, X.Hu, Z.Wang, F.Sun, D.G.Dorrell. *Renew. Sustain. Energy Rev.*, **81**, 1868 (2018)